JOURNAL OF GEOPHYSICAL RESEARCH, VOL. 114, D00F04, doi:10.1029/2008JD011300, 2009

Particulate emissions from commercial shipping: Chemical, physical, and optical properties

Daniel A. Lack,[1,2] James J. Corbett,[3] Timothy Onasch,[4] Brian Lerner,[1,2] Paola Massoli,[1,2] Patricia K. Quinn,[5] Timothy S. Bates,[5] David S. Covert,[6] Derek Coffman,[5] Berko Sierau,[6,7] Scott Herndon,[4] James Allan,[8] Tahllee Baynard,[1,2,9] Edward Lovejoy,[1] A. R. Ravishankara,[1] and Eric Williams,[1,2]

Received 15 October 2008; revised 8 December 2008; accepted 12 December 2008; published 25 February 2009.

[1] We characterize particulate emissions on the basis of chemical, physical, and optical properties from commercial vessels. Observations during the Texas Air Quality Study/Gulf of Mexico Atmospheric Composition and Climate Study 2006 field campaign provide chemical and physical characteristics including sulfate (SO_4^{2-}) mass, organic matter (OM) mass, black carbon (BC) mass, particulate matter (PM) mass, number concentrations (condensation nuclei (CN) > 5 nm), and cloud condensation nuclei (CCN). Optical characterization included multiple wavelength visible light absorption and extinction, extinction relative humidity dependence, and single scatter albedo (SSA). The global contribution of shipping PM was calculated to be 0.90 Tg a^{-1}, in good agreement with previous inventories (0.91 and 1.13 Tg a^{-1} from Eyring et al. (2005a) and Wang et al. [2008]). Observed PM composition was 46% SO_4^{2-}, 39% OM, and 15% BC and differs from inventories that used 81%, 14%, and 5% and 31%, 63%, and 6% SO_4^{2-}, OM, and BC, respectively. SO_4^{2-} and OM mass were found to be dependent on fuel sulfur content as were SSA, hygroscopicity, and CCN concentrations. BC mass was dependent on engine type and combustion efficiency. A plume evolution study conducted on one vessel showed conservation of particle light absorption, decrease in CN > 5 nm, increase in particle hygroscopicity, and an increase in average particle size with distance from emission. These results suggest emission of small nucleation mode particles that subsequently coagulate/condense onto larger BC and OM. This work contributes to an improved understanding of the impacts of ship emissions on climate and air quality and will also assist in determining potential effects of altering fuel standards.

Citation: Lack, D. A., et al. (2009), Particulate emissions from commercial shipping: Chemical, physical, and optical properties *J. Geophys. Res.*, *114*, D00F04, doi:10.1029/2008JD011300.

1. Introduction

[2] The world shipping fleet consists of over 100,000 vessels larger than 100 gross tonnes [*Corbett and Koehler*, 2003], consumes up to 289 million tonnes of fuel per year [*Corbett and Koehler*, 2003; *Endresen et al.*, 2003; *Eyring et al.*, 2005a] and has estimated future growth of 2–6% a^{-1} [*Corbett et al.*, 2006; *Eyring et al.*, 2005b]. Oceangoing ships running large slow-speed diesel (SSD) engines generally burn low-quality residual fuels that tend to contain high amounts of sulfur and heavy metals. Smaller vessels, such as tugboats, fishing vessels and ferries operate medium-speed diesel (MSD) engines that use mostly distillate fuels within nonroad equipment fuel quality standards [*U.S. Environmental Protection Agency*, 2004]. International commercial shipping vessels operate across international waters with little or inconsistent regulation of fuel quality or pollution emissions; domestic fleets serve coastal shipping, resource extraction, harbor service, and vessel assist duties. Aside from CO_2 and H_2O vapor, the expected gas phase products of fuel combustion from shipping (ranked on a mass basis) include nitrogen oxides (NO_X), sulfur dioxide

[1]Chemical Sciences Division, Earth System Research Laboratory, NOAA, Boulder, Colorado, USA.
[2]Also at Cooperative Institute for Research in Environmental Sciences, University of Colorado, Boulder, Colorado, USA.
[3]College of Marine and Earth Studies, University of Delaware, Newark, Delaware, USA.
[4]Aerodyne Research, Inc., Billerica, Massachusetts, USA.
[5]Pacific Marine Environment Laboratory, NOAA, Seattle, Washington, USA.
[6]Atmospheric Sciences Department, University of Washington, Seattle, Washington, USA.
[7]Now at Institute for Atmospheric and Climate Science, Swiss Federal Institute of Technology, Zurich, Switzerland.
[8]National Centre for Atmospheric Science, University of Manchester, Manchester, UK.
[9]Now at Lockheed Martin Coherent Technologies, Louisville, Colorado, USA.

0148-0227/09/2008JD011300$09.00

(SO_2) and carbon monoxide (CO) (E. Williams et al., Emissions of NO_X, SO_2, CO, H_2CO and C_2H_4 from commercial marine shipping during TexAQS 2006, submitted to *Journal of Geophysical Research*, 2008). CO_2 is the most ubiquitous greenhouse gas and emissions from commercial shipping vessels represent ~3.3% of global anthropogenic emissions (excludes CO_2 from land use change) [*Eyring et al.*, 2005a; *Intergovernmental Panel on Climate Change* (IPCC), 2007]. NO_X is a catalyst in tropospheric ozone formation which has both health and climate impacts [*IPCC*, 2007] and shipping contributes ~15–30% to global fossil fuel sourced NO_X emissions [*Corbett et al.*, 2007a]. Commercial shipping is estimated to contribute 5–8% of global anthropogenic SO_2 emissions [*Eyring et al.*, 2005a]. Gaseous oxides of sulfur produced during combustion of fossil fuels can be oxidized to particulate sulfate (SO_4^{2-}). In addition to SO_4^{2-} formed from SO_2, particulate emissions from shipping include BC, organic matter (OM) and ash [*Petzold et al.*, 2004], which include particles of fuel-bound minerals and heavy metals.

[3] Globally, shipping is thought to contribute almost as much primary PM as road traffic (1.7 Tg a^{-1} compared to 2.1 Tg a^{-1} [*Eyring et al.*, 2005a]), including 1.7% of global total BC emissions [*Lack et al.*, 2008a] and 7.5% of fossil and biofuel sourced OM emissions [*Ito and Penner*, 2005; *Wang et al.*, 2008]. (In section 3.3 we show that all light-absorbing carbon (LAC), at 532 nm, is BC. Therefore the terms BC and LAC (used in the *Lack et al.* [2008a] study) can be used interchangeably for this study.) Field observations of the chemical composition of PM emissions from shipping vessels are scarce. *Hobbs et al.* [2000] ruled out BC, SO_4 salts and ammonium nitrate as major contributors to the direct PM from ship emissions; and their results for BC are consistent with engine tests that show high-temperature, high-pressure engines (e.g., large marine engines) are efficient at converting fuel carbon to CO_2. Results of volatility experiments from *Hobbs et al.* [2000] showed that the major components of the PM were high boiling point organics with some sulfuric acid. *Kasper et al.* [2007] and *Petzold et al.* [2008] both found, that after passing PM through a thermal denuder, condensation nuclei (CN) emission factors decreased from 35 to 90% suggesting that much of the PM from marine diesel engines is in the form of externally mixed volatile particles, supporting the findings of *Hobbs et al.* [2000]. *Petzold et al.* [2004] estimated that PM emissions from a marine diesel engine burning heavy fuel oil (HFO) in controlled laboratory conditions (at 25% engine load) contained organic carbon (OC, 7%), SO_4^{2-} (38%), SO_4-bound water (30%), BC (7%) and ash (7%). *Kasper et al.* [2007] measured mass emissions from a two-stroke marine diesel engine burning both residual and distillate marine fuels; that study reported that PM emissions contained ~17% OC and ~17% elemental carbon (EC). *Sax and Alexis* [2007] compiled and reviewed PM mass emission factors from stack tests of marine diesels on oceangoing vessels. They summarized more than 10 unique studies and presented an averaged PM mass-based emission factor for ships burning marine distillate oil (MDO, fuel sulfur content ~0.25%) and HFO (fuel sulfur content ~2.5%). *Sax and Alexis*'s [2007] review reveals large variability in PM mass emissions, with only a weak relationship between PM emissions and fuel sulfur content for HFO-burning vessels. This variability was also demonstrated in the *Lloyd's Register* [1995] study for PM mass and by *Lack et al.* [2008a] for BC emissions.

[4] *Hobbs et al.* [2000], *Petzold et al.* [2008], *Kasper et al.* [2007], *Frick and Hoppel* [2000], and *Durkee et al.* [2000] all investigated size distributions of PM emissions from marine diesel engines and found the majority of particles having diameters from 10 to 100 nm with very few above 250 nm. *Lyyranen et al.* [2002] found additional modes around 2 and 10 μm which formed from heavy metals (i.e., ash) and fuel residue particles respectively. *Lyyranen et al.* [1999] showed that although the size distributions of PM from large and small marine diesel engines were very similar, the absolute magnitude of PM mass from the smaller engines was higher by as much as a factor of two.

[5] Emissions from commercial shipping vessels contribute significantly to perturbations in air quality, visibility and climate. The link between PM emissions and health effects was recently assessed for global shipping emissions when *Corbett et al.* [2007b] estimated that up to 60,000 premature deaths result annually. The primary reason for the efficacy of shipping emissions to health is because 70% of shipping occurs within 400 km of land [*Corbett et al.*, 2007b; *Wang et al.*, 2008] and major shipping ports are located in areas surrounded by large populations.

[6] Emissions of BC, OM and SO_4^{2-} from shipping perturb the radiation balance because of direct scattering or absorption of radiation. The annual radiative impact of PM emissions from commercial vessels is believed to be a cooling effect. *Schreier et al.* [2006], *Capaldo et al.* [1999], and *Lauer et al.* [2007] concluded that SO_4^{2-} formed from ship-emitted SO_2 is a major contributor to cloud condensation nuclei (CCN) and ship track formation. These tracks have been observed from satellites [*Schreier et al.*, 2007] with decreased cloud droplet effective radius, increased droplet concentrations and increased cloud optical thickness relative to unpolluted clouds [*Devasthale et al.*, 2006]. *Hobbs et al.* [2000] and *Sinha et al.* [2003] measured the fraction of CCN to total PM emissions and found that between 4 and 18% of shipping PM number emissions can contribute CCN. *Schreier et al.* [2007] estimated the globally averaged magnitude of the radiative forcing of ship tracks from satellite imagery to be -0.4 mW m^{-2}. The overall impact of ship tracks and the subsequent dilution of the emissions into the regional environment (which cannot be detected using satellites) has been estimated at -0.11 W m^{-2} and -0.19 to 0.60 W m^{-2} by *Capaldo et al.* [1999] and *Lauer et al.* [2007], respectively. Overall radiative forcing effects must also include the cumulative effect of CO_2 from ships using fossil fuels since the late 19th century, recently estimated to be ~0.046 W m^{-2} in 2007 and projected to grow to between 0.096 and 0.115 W m^{-2} by 2050 [*Buhaug et al.*, 2008].

[7] Fuel quality, engine type (combustion conditions) and vessel activity play major roles in the properties and variability of emissions. An improved understanding of emissions and processing of particles from a cross section of marine fuel types, diesel engine types and ship activity is essential to improve understanding of ship PM characteristics in the atmosphere, and the impact of shipping emissions on health, visibility and climate. Here we describe a

comprehensive data set of chemical, physical and optical properties of the PM emissions from up to 211 commercial shipping vessels that were sampled during the Texas Air Quality Study/Gulf of Mexico Atmospheric Composition and Climate Study (TexAQS/GoMACCS) 2006.

2. Field Observations

2.1. TexAQS/GoMACCS 2006 Study

[8] During August–September 2006 the NOAA research vessel *Ronald H. Brown* (RHB) conducted a research cruise from Charleston, South Carolina to Houston, Texas, with most sampling occurring in the Gulf of Mexico, Galveston Bay and the Houston Shipping Channel. During 37 days of sampling more than 1100 commercial and private marine vessels were encountered. Of the plumes of commercial vessels encountered 211 were of sufficient duration and quality to be included in this analysis. Ship information, including size, commercial type, and speed was gathered from Automated Information System (AIS) broadcasts from each vessel. AIS is a globally implemented collision avoidance system required on all vessels larger than 300 gross tonnes (Gt) where specific data (ship name, position, speed, heading, type, etc.) are transmitted continuously over VHF, up to a range of 12 miles. Unique vessel plumes were identified using a combination of the AIS information and meteorology measured onboard the RHB.

2.2. Instrumentation

[9] The RHB was fitted with instrumentation capable of measuring numerous air quality and climate relevant parameters. To capture sufficient data from the ship plumes, all instrumentation required a time response of <5 s, which limited certain parameters from being measured (e.g., particle size distributions).

2.2.1. Gas Phase

[10] Carbon dioxide (CO_2) was determined via nondispersive infrared spectroscopy (LiCor model LI-7000) and SO_2 was measured via pulsed UV fluorescence (TEII model 43s). (Certain commercial equipment, instruments, or materials are identified in this article in order to adequately specify the experimental procedure. Such identification does not imply recognition or endorsement by the National Oceanic and Atmospheric Administration, nor does it imply that the material or equipment identified is necessarily the best available for the purpose.) Further detail on gas phase instrumentation is given by Williams et al. (submitted manuscript, 2008) and *Bates et al.* [2008]. Fuel sulfur content in percent by mass was estimated by dividing the SO_2 mass emission factors by 20 [*Cooper*, 2003; *Hobbs et al.*, 2000; *Lloyd's Register*, 1995], and is estimated to have an uncertainty of ±10%. For this calculation SO_4^{2-} emissions were converted to SO_2 equivalent and added to the SO_2 emission factors to obtain a more certain estimate of fuel sulfur.

2.2.2. Particulate Phase

[11] All particle chemical, physical and optical instruments were located in one of three laboratory vans and sampled from the common particle inlet mast. Details of this system are reported by *Bates et al.* [2008]. A brief summary is included here. The mast, which extended 5 m above and forward of the particle measurement containers, consisted of a 5 cm diameter inlet nozzle sampling at 1 m^3 min^{-1} and was automatically positioned into the relative wind. The lowest 1.5 m of the mast was heated to reduce the RH to 60 (±5) %. Air was subsampled through 1 μm, 50% cut-diameter impactors at 30 l min^{-1}. For instruments requiring flows less than 30 l min^{-1} the flow was subsampled using isokinetic probes. To avoid sample losses, all tubing connecting instrumentation was routed with conductive tubing and minimal sharp bends. All parameters are reported at standard temperature and pressure (STP, 273 K, 1013 hPa).

2.2.2.1. Chemical Properties

[12] Chemically classified and size-resolved mass loadings of submicron particles were measured using a high-resolution time-of-flight aerosol mass spectrometer (HR-ToF-AMS) developed at Aerodyne Research, Inc., (Billerica, Massachusetts, USA) [*Allan et al.*, 2003; *DeCarlo et al.*, 2006; *Drewnick et al.*, 2005; *Jayne et al.*, 2000]. For the specific purpose of measuring particulate emissions from ships, the AMS was operated in a rapid MS-only mode. The chemical species measured included NH_4^+, NO_3^- SO_4^{2-} and most organic carbon species but does not include crustal oxides, BC, or sea salt. This is one of the first applications of a rapid data collection technique and was only attempted during concentrated vessel traffic. The AMS was calibrated multiple times during the study according to established procedures [*Allan et al.*, 2003; *Jayne et al.*, 2000; *Jimenez et al.*, 2003]. The average ionization efficiency and instrument sensitivity remained constant with a precision of ±10% during the study. The collection efficiency (CE) of the AMS is related to particle size and phase [*Liu et al.*, 2007; *Matthew et al.*, 2008] and can be estimated by directly comparing PM measurements from the AMS to other mass and number-based measurements (e.g., Scanning Mobility Particle Sizer (SMPS), Particle In Liquid Sampler (PILS)). For this high time resolution study there were no compatible measurements available for direct CE determination. However, on the basis of analyses from the TexAQS/GoMACCS 2006 study (details to be published elsewhere) and from NEAQS 2004 [*Quinn et al.*, 2006], AMS CE for ambient particles is controlled in large part by the phase of the sulfate in the particles. For cases where the ambient sulfate component was acidic (as is in this study), the AMS CE with respect to particle bounce effects was observed to be 1.0. Laboratory studies have shown that the AMS quantitatively (e.g., CE = 1.0) measures the condensed organic material (solid and liquid coatings) on soot particles generated from premixed flames [e.g., *Slowik et al.*, 2007, Figure 13]. Taken together, this information (and that the ship plumes contained only SO_4^{2-}, OM and BC) implies that the AMS CE for the ship particulate emissions measured during this study should be unity and was chosen to be 1.0 for this study. Without direct confirmation of the AMS CE, the mass measured by the AMS represents a reasonable lower limit for the emitted SO_4^{2-} and OM with combined uncertainties for the AMS measured particulate emissions of −10% and +40%.

2.2.2.2. Physical Properties

[13] Air from the sample inlet was supplied to TSI 3025A, TSI3785, TSI3010 and TSI 3760 particle counters. The 3025A, 3785, 3010 and 3760 measure all particles larger than roughly 3, 5, 12 and 13 nm respectively. The counts from the four detectors are referred to here as CN >

3 nm (TSI3025), CN > 5 nm (TSI3785), CN > 12 nm (TSI3010) and CN > 13 nm (TSI3760). The total particle counts from each instrument were recorded every second. The data were filtered to eliminate periods of calibration and instrument malfunction and periods of RHB exhaust contamination (based on relative wind and high CN counts). The "best" filtered values were chosen to represent CN > 13 nm and CN > 5 nm particle concentrations. The best CN > 13 nm values primarily include data from CN > 12 nm and the data from CN > 13 nm were used to fill in periods when the CN > 12 nm were not available. Similarly, the CN > 5 nm values primarily include data from CN > 5 nm and the CN > 3 nm data were used to fill in periods when CN > 5 nm were not available. Reported measurement uncertainties are ±5% for all CN measurements.

[14] A CCN counter (Droplet Measurement Technologies (DMT)) was used to determine CCN concentrations at supersaturations of 0.22, 0.44, 0.65, 0.84, and 1.0%. Details concerning the characteristics of the DMT CCN counter are given by *Roberts and Nenes* [2005] and *Lance et al.* [2006]. A multijet cascade impactor [*Berner et al.*, 1979] with a 50% aerodynamic cutoff diameter of 1 μm was upstream of the CCN counter. Data reported here are for a supersaturation setting of 0.44%. The CCN counter was calibrated before and during the experiment as outlined by *Lance et al.* [2006]. The uncertainty associated with the CCN number concentrations is estimated to be less than ±10% [*Roberts and Nenes*, 2005]. Uncertainty in the instrumental supersaturation is less than ±1% for the operating conditions of this experiment [*Roberts and Nenes*, 2005].

2.2.2.3. Optical Properties

[15] Particle extinction (dry, RH ~ 25%) was measured using a cavity ring-down aerosol extinction spectrometer (CRD-AES [*Baynard et al.*, 2007]) at 1064 nm, 532 nm and 355 nm ($b_{Ext,1064nm}$, $b_{Ext,532nm}$, $b_{Ext,355nm}$). Two additional 532 nm CRD-AES channels were operated at elevated RH (~85%, 75%) and combined with the dry 532 nm channel to calculate the RH dependence of particle extinction. An additional 532 nm channel measured filtered air to determine the interference from gas phase absorbers (e.g., NO_2, O_3) at that wavelength. This signal was subtracted from total extinction and total absorption. Gas phase interference contributed, on average 4% to extinction and 15% to absorption. Reported measurement uncertainties are 1% ($b_{Ext,532nm}$ dry) and ~5% ($b_{Ext,532nm}$ high RH, $b_{Ext,1064nm}$, $b_{Ext,355nm}$) [*Baynard et al.*, 2007].

[16] Particle absorption was measured at 532 nm ($b_{Abs,532nm}$) using a photoacoustic aerosol spectrometer (PAS [*Lack et al.*, 2006]). Gas phase absorption was removed as described above and most of the PAS data set was described by *Lack et al.* [2008a], taking the form of BC mass emissions, which can be derived from particle light absorption measurements. Particle absorption was also measured using a three-wavelength particle soot absorption photometer (PSAP; Radiance Research Inc., USA) at 670 nm, 530 nm and 440 nm ($b_{Abs,670nm}$, $b_{Abs,530nm}$, $b_{Abs,440nm}$). PSAP data were corrected for filter surface area, flow calibrations and filter transmission according to *Bond et al.* [1999], an additional filter spot size correction [*Sheridan et al.*, 2005] and scattering corrections according to *Virkkula et al.* [2005]. This modified PSAP scheme was applied as a result of the commercial three wavelength PSAP having different geometry than the one used in the *Virkkula et al.* [2005] study. Reported measurement uncertainties are ±5% ($b_{Abs,532nm}$) and ±20% ($b_{Abs,660nm}$, $b_{Abs,530nm}$, $b_{Abs,440nm}$).

2.3. Calculating Emission Factors

[17] Emission factors for the chemical, physical and optical properties of the shipping plumes were calculated using the CO_2 balance method [*Hobbs et al.*, 2000]. This method removes any background contributions (background defined as the preship and postship plume concentrations of the measured species) and accounts for plume dilution. Emission factors for OM, SO_4^{2-}, NH_4^+ and NO_3^- (EF_{OM}, EF_{SO4}, EF_{NH4}, EF_{NO3}) were calculated using equation (1). Emission factors for CN > 13 nm, CN > 5 nm and CCN ($EF_{CN>13nm}$, $EF_{CN>5nm}$, EF_{CCN}) were calculated using equation (2). Emission factors for extinction at 1064 nm, 532 nm and 355 nm ($EF_{Ext,1064nm}$, $EF_{Ext,532nm}$, $EF_{Ext,355nm}$) and absorption at 670 nm, 532 nm, 530 nm and 440 nm ($EF_{Abs,670nm}$, $EF_{Abs,532nm}$, $EF_{Abs,530nm}$, $EF_{Abs,440nm}$) were calculated using equation (3).

$$EF_{Chemical}(g\ kg^{-1}) = \frac{Chemical\ Parameter(\mu g m^{-3})}{CO_2(ppmV)} \times f_{fuel-chemical} \quad (1)$$

$$EF_{Physical}(kg^{-1}) = \frac{Physical\ Parameter(cm^{-3})}{CO_2(ppmV)} \times f_{fuel-physical} \quad (2)$$

$$EF_{Optical}(m^2 kg^{-1}) = \frac{Optical\ Parameter(Mm^{-1})}{CO_2(ppmV)} \times f_{fuel-optical} \quad (3)$$

The conversion factors $f_{fuel-chemical}$ (1.62 g μg m^3 ppmv kg^{-1}), $f_{fuel-physical}$ (1.62 × 10^{12} cm^3 ppmv kg^{-1}) and $f_{fuel-optical}$ (1.62 m^2 ppmv Mm kg^{-1}) convert concentrations of the parameters in air to concentrations per unit fuel burnt and includes (1) the fraction of fuel that is carbon (0.865 by weight [*Lloyd's Register*, 1995]) and (2) the conversion of CO_2 mixing ratio to concentration of carbon. Conversion of EF_{Abs} to EF_{BC} is achieved using a mass absorption coefficient, at 532 nm, of 7.75 m^2 g^{-1} [*Bond and Bergstrom*, 2006]. The precision of the emission factor is calculated to be 8% [*Lack et al.*, 2008a]. Other uncertainties in the calculated quantities include the standard deviation in the ratio between the measured parameter and CO_2 (on average ±10%), uncertainty in fuel carbon content (±1%) and total carbon conversion to CO_2 (±2%). The uncertainty in converting EF_{Abs} to EF_{BC} is ±15.5% [*Lack et al.*, 2008a]. Combined these uncertainties give a total uncertainty in emission factors of approximately ±13% for all but EF_{BC}, which has an uncertainty of approximately ±20%, and $EF_{Chemical}$ which is in the order of ±20%. Figure 1 shows particle extinction (3 RH levels) and CO_2 time series and regressions for a representative ship plume. All chemical, physical and optical properties were analyzed in this way. Emission factors were included in this analysis if the R^2 for the regression of the various parameters with CO_2 was above 0.85. Insufficient data points or low signal levels contribute to rejection of a plume based on these criteria.

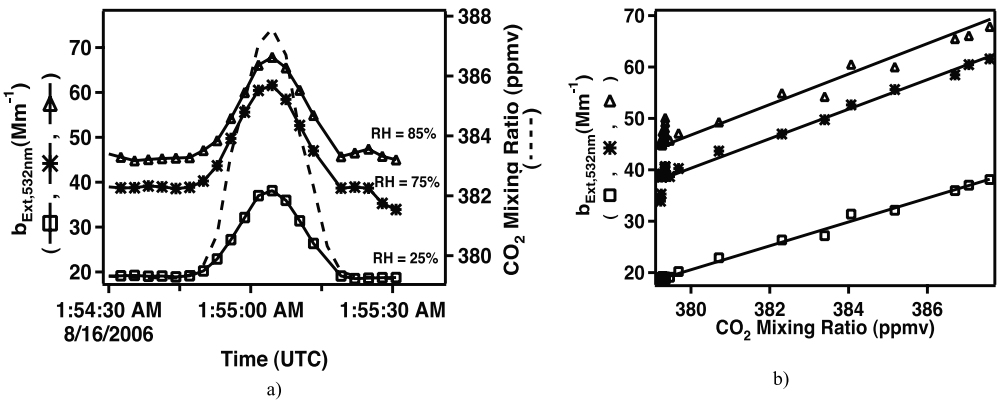

Figure 1. (a) Representative time series of CRD-AES extinction ($b_{Ext,532nm}$) for low, medium, and high RH levels and CO_2 measured in a ship plume. (b) Regression analysis of $b_{Ext,532nm}$ and CO_2 data for all RH levels. RH dependence of extinction calculated using these three slopes and equation (6). All emission factors were calculated in this manner.

[18] One aspect to consider when reporting emission factors is whether the measured parameter is conserved as the plume evolves [*Petzold et al.*, 2008]. For example particle number concentrations will not be conserved downwind of emission as particles coagulate and are removed through deposition. *Petzold et al.* [2008] used the term "effective emission indices" for emissions that were not conserved downwind of emission. We maintain the term "emission factor" for all parameters as it cannot be determined which of the emitted species, if any, are entirely conserved downwind of emission. For this study we consider any nonconservation of the parameter in terms of particle processing and utilize this change as an investigative tool. It remains that field observations of emissions in the environment will not be true emission factors if any transformation occurs (through coagulation, deposition or chemical processing).

2.4. Optical Intensive Properties

[19] Intensive particle optical parameters were calculated using the STP emission factors from the shipping plumes rather than the direct measurement itself. This approach removes any contribution of background particles and dilution from the calculated parameter. As such, all equations below show the emission factors as contributing parameters.

[20] The wavelength (λ) dependence of particle extinction and absorption was calculated according to equation (4), which describes the Ångström exponent (Å).

$$\mathring{A}_{optical,\lambda 1,\lambda 2} = -\frac{\ln\left(EF_{optical,\lambda 1} \Big/ EF_{optical,\lambda 2}\right)}{\ln\left(\lambda_1 \Big/ \lambda_2\right)} \quad (4)$$

The widest wavelength range for extinction Å was 355 nm to 1064 nm ($\mathring{A}_{Ext,355nm,1064nm}$) while for absorption it was 440 nm to 670 nm ($\mathring{A}_{Abs,440nm,670nm}$). All other wavelength combinations are included in this analysis. Ångström exponents for extinction give an indication of particle size, specifically $\mathring{A}_{Ext,355nm,1064nm} > 2$ indicates dominance of particles smaller than 100 nm, while $\mathring{A}_{Ext,355nm,1064nm} < 1$ indicates dominance of particles larger than 500 nm [*Schuster et al.*, 2006]. Ångström exponents for absorption give an indication of the contribution of absorbers other than BC, with $\mathring{A}_{Abs} \sim = 1$ indicating mostly BC, while $\mathring{A}_{Abs} > 1$ tend to indicate organic matter or dust absorbing in the blue/UV wavelengths [*Bergstrom et al.*, 2007; *Kirchstetter et al.*, 2004].

[21] Particle single scattering albedo at 532 nm (ω_{532nm}) was derived from CRD-AES extinction and PAS absorption according to equation (5).

$$\omega_{532nm} = \frac{EF_{Ext,532nm} - EF_{Abs,532nm}}{EF_{Ext,532nm}} \quad (5)$$

The RH dependence of extinction of atmospheric particles can be described by Gamma ($\gamma_{Ext,532nm}$) [*Quinn et al.*, 2005]. Gamma is the slope of the regression of multiple extinction terms measured at various RH levels versus these RH terms (equation (6)).

$$\gamma_{Ext,532nm} = \frac{\log(EF_{Ext,532nm})}{2 - \log(100 - RH)} \quad (6)$$

3. Results

3.1. Overview

[22] The study area, cruise track of the RHB and the locations of most encounters with shipping vessels during the study is shown in Figure 2a. This study captures the diversity and distribution of vessel types within the global fleet (Figure 2b) [adapted from *Corbett and Koehler*, 2003] although we recognize that the sampling region does contain, and should be expected to contain, regional differences from the global composition. For example cargo and bulk ships are under sampled in this region compared to the global average. Vessels classified as "other" include fishing vessels, tugboats and ferries. The parameters and symbols used for each measurement and the emission factors derived from that measurement are summarized in Table 1. Table 2 contains averages of the measured chemical, physical and

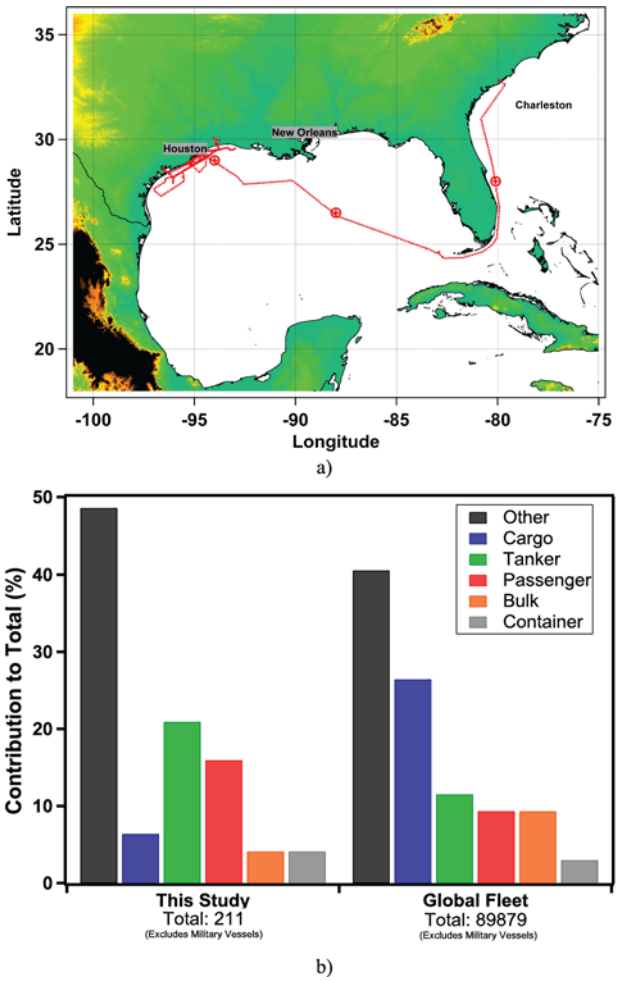

Figure 2. (a) Map of study area, showing regions of most shipping vessel encounters (red symbols). (b) Distribution of vessel numbers by class sampled in this study and for the global fleet [*Corbett and Koehler*, 2003]. "Other" includes tugboats, ferries, large fishing vessels, etc. Excludes military vessels.

optical properties averaged for (1) all vessels, (2) vessels equipped with SSD engines, (3) vessels equipped with MSD engines, (4) vessels burning high-sulfur fuel, and (5) vessels burning low-sulfur fuel. It must be noted that most often SSD vessels burn high-sulfur fuel and MSD vessels burn low-sulfur fuel, however this is not always the case. Classification of categories 1 and 2 was derived from the AIS information and from the *Lloyd's MIU* [2006] directory while calculated fuel sulfur content, derived as noted above, was used to classify categories 4 and 5.

[23] The following details are reiterated: (1) all sampling was carried out behind a 1 μm cut point impactor, so contributions of larger particles were not measured; (2) the method of calculating emission factors removes any contribution of background PM; and (3) unitless emission factors are in fact intensive properties of the PM emissions with the background contribution removed.

3.2. Particle Composition

[24] Shipping emissions were found to contain exclusively SO_4^{2-}, OM and BC (Table 2). Ash is likely the only emission that could not be measured in this study and is thought to comprise a few percent of total mass emissions [*Petzold et al.*, 2004]. Emitted SO_4^{2-} is very likely sulfuric acid indicated by the absence of NH_4^+ or NO_3^-. SSD vessels are emitting more than twice as much SO_4^{2-} and OM compared to MSD and high-speed diesel (HSD) vessels (Table 3) while MSD vessels emit more than twice as much BC as SSD and HSD vessels (*Lack et al.* [2008a] and Table 3). Unlike BC emissions, SO_4^{2-} and OM emissions are of similar quantity among other vessel classes. Table 3 also shows a breakdown of measured SO_4^{2-}, OM and BC emission factors for vessel commercial classification (i.e., tanker, container, cargo and bulk ships and tug and passenger boats). We emphasize that these emission factors are for emissions up to ~15 min downwind of the exhaust stack. SO_4^{2-} generally is not emitted directly from these engines, but forms after release from the stack. As a result, reported emission factors for SO_4^{2-} derived from this study are for "freshly formed" emissions and the eventual mass of SO_4^{2-} formed from vessel emissions may be higher.

3.3. Particle Absorption and Composition

[25] The OM component of the emissions is shown to be non–light absorbing at visible wavelengths (Figure 3a), which provides some insights to the OM composition. The wavelength dependence of absorption ($\mathring{A}_{Abs}$) of pure BC is expected to be unity. *Kirchstetter et al.* [2004] and *Lewis et al.* [2008] showed that some OM emitted by biomass combustion have a spectral dependence of light absorption that is stronger than that due to BC (i.e., $\mathring{A}_{Abs} > 1$). As shown in Table 2 and Figure 3a, $\mathring{A}_{Abs}$ averaged 0.98 (±0.20) for all wavelength combinations indicating that the majority of OM from shipping emissions does not absorb light at the visible wavelengths of the PSAP. As a result the terms "BC" and "light-absorbing carbon" (LAC) are interchangeable for this study. We also show that the PSAP and PAS (at 532 nm) are comparable to within the uncertainties of the instrumentation (PSAP = 20%, PAS = 5%) (Figure 3b, slope (R_{Abs}) of 1.1), which addresses concerns about potential biases in the PSAP [*Lack et al.*, 2008b].

3.4. Particle Number Concentrations

[26] On average SSD engines produce more particles ($EF_{CN>5nm}$) than MSD engines (Table 4). This is consistent with SSD engines running at higher temperatures and pressures that are combustion conditions favorable to the production of higher number concentrations [*Heywood*, 1988]. The average $EF_{CN>5nm}$ (total CN) for all vessels encountered is 1.27 (±0.95) × 10^{16} particles kg^{-1} (Table 2). Up to 4 min downwind of emission nucleation mode particles (<13 nm) dominate number concentrations (Figure 4). After approximately 4 min most particles are >13 nm, presumably because of growth by coagulation. Figure 4 shows that nucleation mode particles (5–13 nm) can exceed the Aitken mode (>13 nm) by up to 10 times just after emission, however most particles are within the Aitken mode soon after 4 min from emission. This result is consistent with emission or very fast formation of small sulfuric acid particles, which then coagulate with the larger OM and BC. It is also observed that the relative contributions of nucleation mode particles to the total are independent of engine type. Table 4 also summarizes emission

Table 1. Summary of Parameters Measured and Corresponding Symbols

Parameter	Parameter/Emission Factor Symbol	Units
	Chemical	
Aerosol mass concentration		
Organic matter	OM/EF_{OM}	g kg^{-1}
Sulfate	SO_4^{2-}/EF_{SO4}	g kg^{-1}
Sulfur as sulfate	$f_{S\ as\ SO4}$	%
Ammonium	NH_4/EF_{NH4}	g kg^{-1}
Nitrate	NO_3/EF_{NO3}	g kg^{-1}
SO_4^{2-} + OM + NH_4^+ + NO_3^-	Total AMS/EF_{AMS}	g kg^{-1}
Black carbon	BC/EF_{BC} [*Lack et al.*, 2008a]	g kg^{-1}
SO_4^{2-} + OM + NH_4^+ + NO_3^- + BC	AMS + BC/EF_{AMS+BC}	g kg^{-1}
	Physical	
Particle number concentration		
>13 nm diameter	CN > 13 nm/$EF_{CN>13nm}$	kg^{-1}
>5 nm diameter	CN > 5 nm/$EF_{CN>5nm}$	kg^{-1}
Cloud condensation nuclei	CCN/EF_{CCN}	kg^{-1}
CN >5 nm as CCN	$f_{CN\ as\ CCN}$	%
	Optical	
Extinction		
355 nm	$b_{Ext,355nm}/EF_{Ext,355nm}$	m^2 kg^{-1}
532 nm	$b_{Ext,532nm}/EF_{Ext,532nm}$	m^2 kg^{-1}
1064 nm	$b_{Ext,1064nm}/EF_{Ext,1064nm}$	m^2 kg^{-1}
RH dependence: 532 nm	$\gamma_{Ext,532nm}$	
Absorption		
440 nm	$b_{Abs,440nm}/EF_{Abs,440nm}$	
530 nm	$b_{Abs,530nm}/EF_{Abs,530nm}$	m^2 kg^{-1}
532 nm	$b_{Abs,532nm}/EF_{Abs,532nm}$	m^2 kg^{-1}
670 nm	$b_{Abs,670nm}/EF_{Abs,670nm}$	m^2 kg^{-1}
Albedo 532 nm	ω_{532nm}	m^2 kg^{-1}
Angstrom exponent		
Extinction, 355 nm: 532 nm	$\mathring{A}_{Ext,355nm,532nm}$	
Extinction, 355 nm: 1064 nm	$\mathring{A}_{Ext,355nm,1064nm}$	
Extinction, 532 nm: 1064 nm	$\mathring{A}_{Ext,532nm,1064nm}$	
Absorption, 440 nm: 530 nm	$\mathring{A}_{Abs,440nm,530nm}$	
Absorption, 440 nm: 670 nm	$\mathring{A}_{Abs,440nm,670nm}$	
Absorption, 530 nm: 670 nm	$\mathring{A}_{Abs,530nm,670nm}$	

factors reported in previous studies and shows that our reported emission factors tend to be at the lower boundary for those studies, although they compare well to the most recent study of *Petzold et al.* [2008].

3.5. Effect of Fuel Sulfur on Particulate Emissions

[27] The following sections present data for which significant correlations were found between measured parameters and fuel sulfur content. Here it is important to consider that most diesel engine systems are designed to maintain high-exhaust gas flows and temperatures to reduce formation of SO_3 to a few percent and avoid water condensation temperatures [*Heywood*, 1988; *Stinson*, 1990; *Turns*, 1996]. The operation of engines in this manner minimizes corrosive exhaust gases and allows fuel sulfur to be emitted almost exclusively as SO_2, which means that sulfur-containing aerosols are generally formed following release from the stack.

3.5.1. Fuel Sulfur and Particle Composition

[28] Emissions of SO_4^{2-} and OM appear linearly correlated with fuel sulfur content (Figures 5a and 5b) while emissions of BC appear inversely correlated to fuel sulfur content (Figure 5c). The SO_4^{2-} relationship is expected while the relationship observed between OM and fuel sulfur may be explained by the consumption rates of cylinder lubricating oils. Engines consume cylinder lubricating oil, in part to help neutralize the corrosive products formed from the fuel sulfur [*Heywood*, 1988]. Consumption rates of lubricating oil are somewhat dependent on the fuel sulfur content and the quantity of oil available to the engine (larger engines have larger sump volumes) [*Kittiwake*, 2008]. Consumption of these specially designed oils will be observed within the PM emissions as OM; therefore, OM will be related to both fuel sulfur content and engine type. The inverse relationship between BC and fuel sulfur is a secondary one and is in fact primarily due to the operating conditions of each engine type. BC emissions are heavily dependent on engine type and are constant for SSD engines and highly variable for MSD engines (also presented by *Lack et al.* [2008a, Figures S1c and S1d]). Some studies have assumed that most PM emissions are a result of the fuel sulfur forming sulfuric acid droplets and SO_4^{2-} particles and these studies seek a correlation between total PM mass emissions to fuel sulfur content [*Lloyd's Register*, 1995; *Sax and Alexis*, 2007]. This assumption seems to be justified on first principles of combustion and when considering inventory assumptions of *Eyring et al.* [2005a] (shown in Figure 11a) who estimated that SO_4^{2-} contributes 81% of PM mass. The data presented here show that both SO_4^{2-} and OM are related to fuel sulfur content and explain the weaker than expected relationship between PM mass and fuel sulfur content of *Sax and Alexis* [2007].

3.5.2. Fuel Sulfur and Particle Size

[29] Figure 6 suggests that high sulfur containing fuels produce more small particles than low sulfur containing fuels. The extinction Angstrom exponent ($\mathring{A}_{Ext,355nm,1064nm}$)

Table 2. Averaged Emission Factors for All Plumes, Slow- and Medium-Speed Diesel Engine Vessels, and High- and Low-Sulfur Fuel Burning Vessels

Emission Factor	All Plumes (Number of Data Points)	SSD (Number of Data Points)	MSD (Number of Data Points)	>0.5% Sulfur (Number of Data Points)	<0.5% Sulfur (Number of Data Points)	Units
			Mass			
EF_{SO4}	1.21 ± 1.50 (43)	1.5 ± 1.6 (29)	0.6 ± 0.4 (12)	2.1 ± 1.6 (23)	0.06 ± 0.05 (15)	g kg^{-1}
EF_{OM}	1.26 ± 0.96 (43)	1.5 ± 1.0 (29)	0.7 ± 0.4 (12)	1.6 ± 0.7 (23)	0.9 ± 1.2 (15)	g kg^{-1}
$f_{S\ as\ SO4}$	2.85 ± 2.10 (43)	3.3 ± 2.3 (24)	1.6 ± 1.0 (9)	3.9 ± 2.0 (19)	1.4 ± 1.1 (14)	%
EF_{NH4}	0.0 ± 0.1 (43)	0.0 ± 0.1 (29)	0.0 ± 0.1 (12)	0.0 ± 0.1 (23)	0.0 ± 0.1 (15)	g kg^{-1}
EF_{NO3}	0.0 ± 0.1 (43)	0.0 ± 0.1 (29)	0.0 ± 0.1 (12)	0.0 ± 0.1 (23)	0.0±0.1 (15)	g kg^{-1}
EF_{AMS}	2.47 ± 2.04	2.9 ± 2.1 (29)	1.3 ± 1.3 (12)	3.6 ± 1.9 (23)	0.9 ± 1.3 (15)	g kg^{-1}
EF_{BC} [*Lack et al.*, 2008a]	0.85 ± 0.76 (100)	0.7 ± 0.8 (52)	1.0 ± 0.7 (51)	0.5 ± 0.5 (42)	1.1 ± 0.8 (53)	g kg^{-1}
EF_{AMS+BC}	3.32 ± 4.04 (43)	3.0 ± 1.7 *(8)*	2.5 ± 1.4 (7)	3.3 ± 1.4 (10)	1.8±1.4 (5)	g kg^{-1}
			Physical			
$EF_{CN>13nm}$	0.71 (±0.55) × 10^{16} (172)	0.8 (±0.5) × 10^{16} (93)	0.6 (±0.5) × 10^{16} (72)	1.0 (±0.5) × 10^{16} (67)	0.5 (± 0.4) × 10^{16} (84)	kg^{-1}
$EF_{CN>5nm}$	1.27 (±0.95) × 10^{16} (165)	1.4 (±1.0) × 10^{16} (87)	1.1 (±0.8) × 10^{16} (72)	2.0 (±1.0) × 10^{16} (60)	1.0 (± 0.7) × 10^{16} (83)	kg^{-1}
EF_{CCN}	0.16 (±0.20) × 10^{16} (113)	0.24 (±0.20) × 10^{16} (58)	0.05 (±0.03) × 10^{16} (51)	0.3 (±0.2) × 10^{16} (47)	0.02 (± 0.01) × 10^{16} (50)	kg^{-1}
$f_{CN\ as\ CCN}$	13.1 (±11.1) (100)	33.9 ± 27.3 (58)	9.4 ± 6.4 (50)	42.0 ± 24.7 (51)	7.4 ± 6.0 (55)	%
			Optical (25% RH)			
Extinction						
$EF_{Ext,355nm}$	27.7 ± 16.4 (57)	28.0 ± 17.0 (29)	27.2 ± 15.8 (24)	29.8 ± 16.0 (20)	27.9 ± 17.3 (32)	$m^2\ kg^{-1}$
$EF_{Ext,532nm}$	9.7 ± 6.2 (94)	8.7 ± 5.4 (50)	11.3 ± 6.7 (39)	7.4 ± 3.3 (38)	12.1 ± 6.9 (42)	$m^2\ kg^{-1}$
$EF_{Ext,1064nm}$	3.4 ± 2.9 (57)	2.6 ± 2.6 (29)	4.5 ± 3.0 (24)	2.1 ± 2.7 (20)	4.4 ± 2.9 (32)	$m^2\ kg^{-1}$
$\gamma_{Ext,532nm}$	0.53 ± 0.45 (56)	0.66 ± 0.47 (35)	0.23 ± 0.18 (16)	0.73 ± 0.46 (32)	0.18 ± 0.09 (17)	
Absorption						
$EF_{Abs,440nm}$	9.7 ± 7.9 (24)	10.0 ± 7.4 (9)	9.5 ± 8.6 (14)	7.0 ± 6.8 (7)	11.3 ± 8.4 (15)	$m^2\ kg^{-1}$
$EF_{Abs,530nm}$	8.3 ± 7.0 (24)	8.5 ± 6.5 (9)	8.2 ± 7.4 (14)	5.8 ± 5.8 (7)	9.8 ± 7.3 (15)	$m^2\ kg^{-1}$
$EF_{Abs,532nm}$	7.5 ± 5.8 (109)	5.6 ± 6.3 (52)	7.6 ± 5.2 (51)	3.8 ± 4.2 (42)	8.8 ± 6.3 (53)	$m^2\ kg^{-1}$
$EF_{Abs,670nm}$	6.6 ± 5.7 (24)	6.7 ± 5.3 (9)	6.6 ± 5.9 (14)	4.4 ± 4.6 (7)	7.9 ± 5.7(15)	$m^2\ kg^{-1}$
ω_{532nm}	0.37 ± 0.22 (75)	0.55 ± 0.21 (35)	0.35 ± 0.18 (33)	0.60 ± 0.21 (31)	0.35 ± 0.17 (33)	
Angstrom exponent						
$\mathring{A}_{Ext,355nm,532nm}$	2.56 ± 1.30 (54)	3.0 ± 1.2 (28)	2.0 ± 1.3 (23)	3.4 ± 1.3 (20)	2.1 ± 1.1 (30)	
$\mathring{A}_{Ext,355nm,1064nm}$	2.10 ± 0.73 (58)	2.3 ± 0.6 (29)	1.8 ± 0.7 (26)	2.6 ± 0.7 (19)	1.8 ± 0.5 (33)	
$\mathring{A}_{Ext,532nm,1064nm}$	1.87 ± 0.96 (54)	2.2 ± 1.0 (28)	1.5 ± 0.7 (23)	2.4 ± 1.2 (20)	1.5 ± 0.6 (30)	
$\mathring{A}_{Abs,440nm,530nm}$	0.93 ± 0.25 (24)	1.1 ± 0.3 (9)	0.8 ± 0.2 (14)	1.2 ± 0.2 (7)	0.8 ± 0.2 (16)	
$\mathring{A}_{Abs,440nm,670nm}$	0.98 ± 0.20 (24)	1.1 ± 0.2 (9)	0.90 ± 0.1 (14)	1.2 ± 0.2 (7)	0.9 ± 0.1 (16)	
$\mathring{A}_{Abs,530nm,670nm}$	1.02 ± 0.19 (24)	1.1 ± 0.2 (9)	1.0 ± 0.1 (14)	1.2 ± 0.2 (7)	0.9 ± 0.1 (16)	

Table 3. Particle Composition Emission Factors by Vessel Category

Vessel Engine Classification	SO_4^{2-} (g kg^{-1}) Average ±S.D.	Data Points	OM (g kg^{-1}) Average ± S.D.	Pnts	BC (g kg^{-1}) Average ± S.D.	Pnts
Slow-speed diesel (SSD)	1.55 ± 1.10	28	1.57 ± 0.83	28	0.41 ± 0.27	42
Medium-speed diesel (MSD)	0.79 ± 0.70	12	0.65 ± 0.44	12	0.97 ± 0.66	51
High-speed diesel (HSD)	0.53 ± 0.46	3	0.75 ± 0.22	3	0.36 ± 0.23	8
Vessel type						
Tankers (SSD)	1.42 ± 1.36	20	1.42 ± 0.98	20	0.38 ± 0.27	31
Container (SSD)	3.58 ± 3.20	3	2.10 ± 0.92	3	0.80 ± 0.23	4
Cargo carriers (SSD)	-	0	-	0	0.40 ± 0.23	4
Bulk carriers (SSD)	0.79 ± 0.70	5	1.90 ± 1.26	5	0.38 ± 0.16	3
Tug boats (MSD)	0.60 ± 0.98	12	0.65 ± 0.44	12	0.97 ± 0.66	51
Passenger boats (HSD)	0.53 ± 0.46	3	0.75 ± 0.22	3	0.36 ± 0.23	8

can provide an estimate of average particle size where an $\mathring{A}_{Ext,355nm,1064nm} > 2$ indicates a size distribution dominated by fine mode particles (e.g., <100 nm), usually from combustion sources whereas $\mathring{A}_{Ext,355nm,1064nm} < 1$ indicates a size distribution dominated by larger sizes (e.g., >500 nm) [*Schuster et al.*, 2006]. An average $\mathring{A}_{Ext,355nm,1064nm}$ for this study of 2.10 (median = 2.0) indicates that, as expected, the combustion emissions from shipping are dominated by fine mode particles. This indirect indication of particle size is consistent with previous studies that directly measured particle size distributions [*Durkee et al.*, 2000; *Frick and Hoppel*, 2000; *Hobbs et al.*, 2000; *Kasper et al.*, 2007; *Petzold et al.*, 2008]. Some size change within Figure 6 will be explained by downwind processing, examples of which are shown in Figures 4 and 10c, which accounts for some of the spread in the data. There are at least two processes contributing to the size distribution of the emitted particles. First, nucleation mode particles (e.g., sulfuric acid) can be emitted from, or formed immediately following combustion, as *Petzold et al.* [2008] suggested and as appears to be the case in the data presented here (Figure 4). Second, different engine sizes burning the same fuel appear to emit very similar size distributions as shown by *Lyyranen et al.* [1999]. This distribution serves as the base for coagulation of the nucleation mode particles formed from the fuel sulfur.

3.5.3. Fuel Sulfur and Particle Single Scattering Albedo

[30] Particles emitted from vessels burning low-sulfur fuels are highly light absorbing with ω_{532nm} values (reported for 25% RH) ranging from ~0.15–0.50 while vessels burning high-sulfur fuels emit a higher proportion of scattering material (ω_{532nm} up to ~0.8) (Figure 7). The lowest ω_{532nm} are consistent with those measured for poly disperse flame generated BC and diesel BC [*Schnaiter et al.*, 2003]. Higher ω values measured in poly disperse atmospheric particles are due to the presence of non-BC scattering material, such as SO_4^{2-} and OM. Both SSD and MSD engines emit PM with a wide range of ω_{532nm} that generally decreases as fuel sulfur content decreases (Figure 7). This observed relationship between ω_{532nm} and fuel sulfur content provides further confirmation that sulfur-containing particles are formed very soon after the combustion process. The wide range of ω_{532nm} from 0.1 to 0.6 for MSD may be an indication (1) of emission of other scattering material, such as unburned lubricating oils [*Hobbs et al.*, 2000], (2) of the variable loads and corresponding exhaust temperatures typical of those vessels (tugs, ferries, etc.), or (3) that some of these ship engines are tuned for power (higher-temperature cylinder combustion) while some are tuned for economy (lower average cylinder temperatures and pressures).

3.5.4. Fuel Sulfur and Particle Relative Humidity Dependence

[31] The hygroscopicity of particles emitted from ships is dependent on fuel sulfur content (Figure 8). The hygroscopicity of the particle emissions can be represented by the RH dependence of particle extinction (presented as $\gamma_{Ext,532nm}$). As RH increases, particles absorb water and their surface areas (and thus extinction) increase. Figure 8 suggests (as expected) that the SO_4^{2-} is responsible for the hygroscopicity of the PM. The effect on hygroscopicity has potential impacts on the lifetime of the particle. Particle water uptake influences a particle's ability to act as a CCN and thus makes it more likely to be processed into clouds and eventually precipitate out of the atmosphere. As fuel

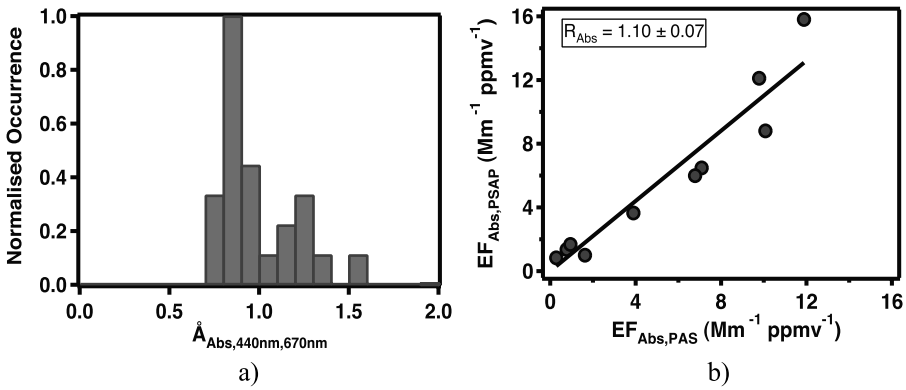

Figure 3. (a) Frequency distribution of PSAP-measured $\mathring{A}_{Abs,440nm,670nm}$. (b) Comparison of PSAP and PAS measured absorption emission factors (532 nm).

Table 4. Summary of Emission Factors of Particle Number Concentrations from this Study for Various Marine Diesel Engines[a]

Reference	Total: $EF_{CN>5nm}$ (kg^{-1})	SSD: $EF_{CN>5nm}$ (kg^{-1})	MSD: $EF_{CN>5nm}$ (kg^{-1})
This study	$1.27 (\pm 0.95) \times 10^{16}$	$2.71 (\pm 1.08) \times 10^{16}$	$1.08 (\pm 0.68) \times 10^{16}$
Petzold et al. [2008]		1.36×10^{16}	
Hobbs et al. [2000]		2.10×10^{16}	1.45×10^{16}
Chen et al. [2005]		$4.65 (\pm 1.80) \times 10^{16}$	
Sinha et al. [2003]		5.1×10^{16}	
Kasper et al. [2007], *Petzold et al.* [2008]		$0.5-4 \times 10^{16}$	
E. Williams (unpublished data, 2008)[b]		1.01×10^{16}	

[a]Also included is a comparison to other studies. Uncertainty given is variability between different vessels rather than measurement precision.
[b]From 2004 NEAQS study. Intercept of large container ship.

sulfur content is decreased it is likely that PM emissions will have longer lifetimes due to reduction in hygroscopic behavior. This lifetime will increase to the extent dictated by the proximity to, and processing within other air masses that can convert the nonhygroscopic shipping PM to a hygroscopic form. Within the marine boundary layer, other sources of hygroscopic material will include sea salt and SO_4^{2-} from dimethyl sulfide [*Bates et al.*, 1992]. In the urban environment hygroscopic material will arise from SO_4^{2-} from other anthropogenic emissions.

3.5.5. Fuel Sulfur and Cloud Condensation Nuclei

[32] A positive correlation between CCN and fuel sulfur is shown in Figure 9. Although this relationship is expected, assessments of the cloud nucleating ability of shipping emissions are very limited which contributes to the large uncertainty reported for the radiative forcing from ships [*Capaldo et al.*, 1999; *Lauer et al.*, 2007; *Schreier et al.*, 2007]. *Sinha et al.* [2003] and *Hudson et al.* [2000] reported CCN to CN ratios ($f_{CN\ as\ CCN}$) of 0.4% to 19% for 12 vessels burning different fuel types (some of this data also included by *Hobbs et al.* [2000]). These appear to be the only direct measurements of CCN from shipping emissions. We measured an average EF_{CCN} of 0.16×10^{16} kg^{-1} which compares well to calculations by *Petzold et al.* [2008] of 0.166×10^{16} kg^{-1}. Figure 9 shows the fraction of total PM

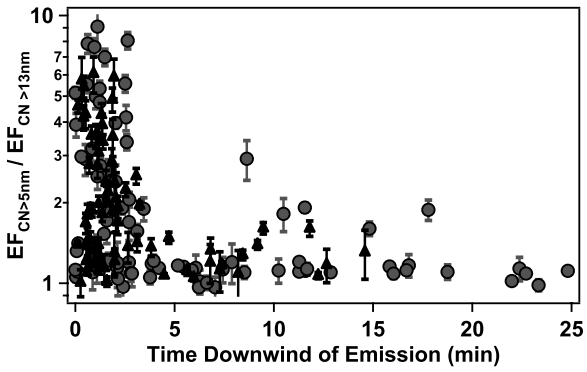

Figure 4. Ratio of $EF_{CN>5nm}$ to $EF_{CN>13nm}$ versus time downwind of emission. The data show that closest to the emission source most particles are CN > 5 nm. After 4 min downwind most 13 nm > CN > 5 nm particles have either coagulated or otherwise grown to CN > 13 nm. Circles indicate SSD vessels, and triangles indicate MSD vessels.

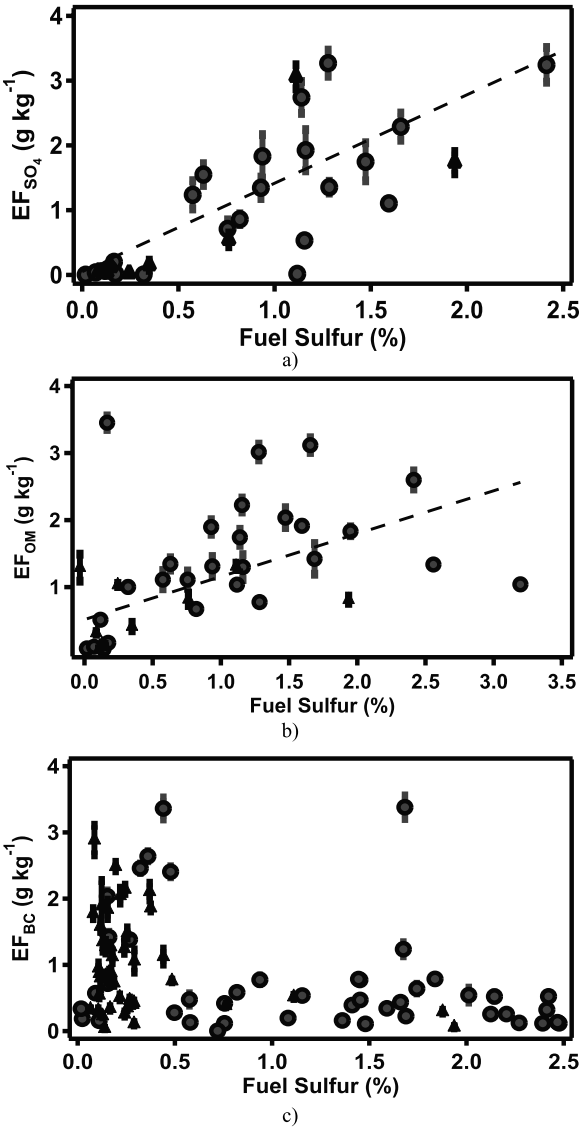

Figure 5. Comparison of (a) SO_4^{2-}, (b) OM, and (c) BC with fuel sulfur content. Circles indicate SSD vessels, and triangles indicate MSD vessels. (SO_4^{2-} slope = 1.4, Int = 0.05, and $R^2 = 0.71$. OM slope = 0.65, Int = 0.5, and $R^2 = 0.62$.)

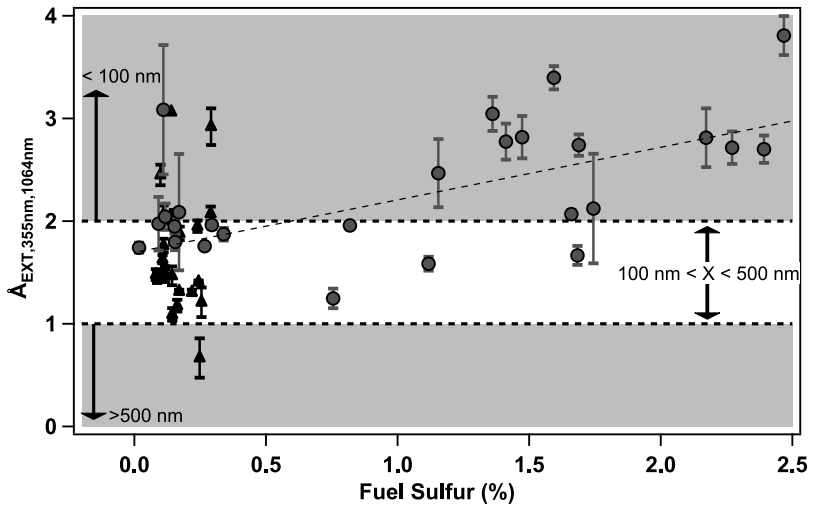

Figure 6. Wavelength dependence of extinction versus fuel sulfur content. Circles indicate SSD vessels, and triangles indicate MSD vessels. Shaded and nonshaded areas indicate approximate average particle size boundaries. (Slope = 0.5, Int = 1.7, and R^2 = 0.64.)

number that can act as CCN, which appears to increase 13% for every 1% increase in fuel sulfur, with very low sulfur fuels producing a minimum of 3% CCN. The existence of CCN without substantial fuel sulfur indicates that a small number of CCN are a result of a highly oxidized PM surface and/or mildly hygroscopic minerals or organics.

3.6. Plume Evolution Study

[33] On 8 August 2006 the RHB sampled downwind of a stationary tanker ship transecting the plume of the stationary vessel on seven occasions (Figure 10a). These intersections occurred at various distances and times downwind (up to 7 min) and offered the opportunity to investigate plume processing and also test the precision of the experimental method.

[34] Figures 10b and 10c show ω_{532nm}, $\gamma_{Ext,532nm}$, $EF_{CN>5nm}$ and $Å_{Ext,355,1064nm}$ for this plume. $\gamma_{Ext,532nm}$ shows a trend toward increasing hygroscopicity with time downwind of emission. The mechanism for this increase is likely the formation of sulfuric acid from gas phase SO_3 and uptake of that material onto existing PM. A $\gamma_{Ext,532nm}$ of 1 indicates a significant amount of water uptake (hydrophobic aerosol will have a $\gamma_{Ext,532nm}$ of $\sim$ 0.2–0.4) and therefore a significant amount of hygroscopic material must be present. The uncertainties of ω_{532nm} make it difficult to assess if ω_{532nm} is increasing with time, which would indicate an increase in the relative amount of scattering particles that are hygroscopic (e.g., SO_4^{2-}). In Figure 10b, ω_{532nm} does appear to be constant, or increasing slightly, as the plume ages. Figure 10c shows that CN > 5 nm concentrations decrease with time downwind of emission; a likely loss through coagulation, indicated by an increase in average particle size, which is evidenced by the decrease in $Å_{Ext,355nm,1064nm}$ downwind of emission. These results are consistent with the results from sections 3.4 and 3.5.2 and point to physical and optical processing of the plume.

[35] Particle absorption provides the best opportunity to assess precision of the methods of calculating the emission factors. Once plume dilution is accounted for, particle absorption should not change significantly within the time-frame of this sampling. This is because more absorbing

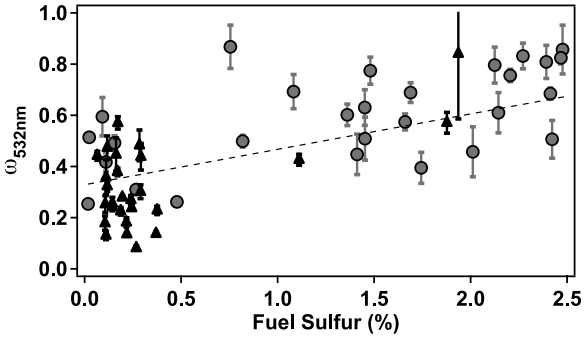

Figure 7. Particle single scattering albedo (at 25% RH) versus fuel sulfur content. Circles indicate SSD vessels, and triangles indicate MSD vessels. (Slope = 0.15, Int = 0.3, and R^2 = 0.60.)

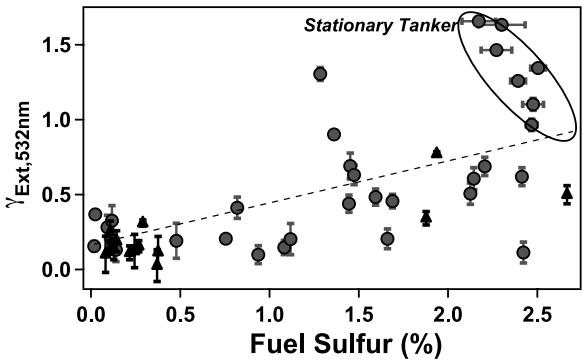

Figure 8. The $\gamma_{EXT,532nm}$ dependence on fuel sulfur content from all vessels. The data points from the stationary tanker encounter (section 3.6) are identified in the ellipse. Uncertainty for fuel sulfur content shown for this encounter only. Circles indicate SSD vessels, and triangles indicate MSD vessels. (Slope = 0.3, Int = 0.2, and R^2 = 0.62.)

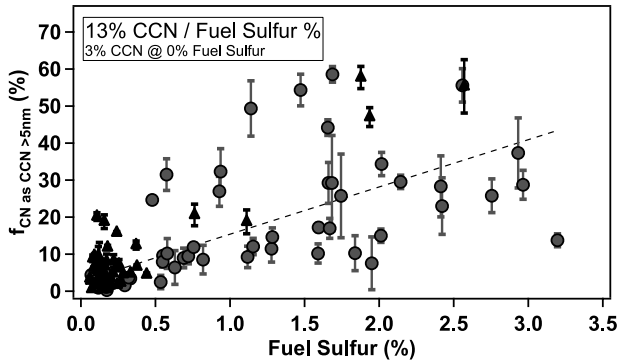

Figure 9. Comparison of the fraction of CN > 5 nm that are CCN with fuel sulfur content. Circles indicate SSD vessels, and triangles indicate MSD vessels. (Slope = 13, Int = 3, and R^2 = 0.66.)

aerosol cannot be formed this quickly (if at all) and enhancement of absorption due to coating of scattering material [*Bond et al.*, 2006] does not appear to be effective within the timeframe of interest. Precision in $b_{Abs,532nm}$ measurements of the tankers plume was less than 8% [*Lack et al.*, 2008a, Figure 1d].

[36] These results show that the variability in measured emission factors observed in this data set is predominantly due to engine type and vessel activity rather than the reproducibility of the measurement techniques or ability to measure the processing of the PM.

4. Discussion

4.1. Estimate of Global PM Contribution

[37] Using the observation-derived emission factors in Table 5 with the global vessel type and fuel usage distributions (for 2001) from *Eyring et al.* [2005a], which is in close agreement with the recent inventory of *Wang et al.* [2008], we calculate a total global annual particle mass from shipping of 0.90 Tg a^{-1}. This assessment includes mass from direct emissions of SO_4^{2-} (46%), OM (39%) and BC (15%) only. According to *Petzold et al.* [2004] direct particle emissions from ships contain SO_4^{2-} (38%), OM (18%), BC (7%), SO_4-bound water (30%) and ash (7%). In this study we did not have the capabilities to measure ash and do not consider SO_4-bound water to be a direct emission from marine engines. To enable a comparison between our assessment and other inventories we remove the contribution of SO_4-bound water and ash from the results of *Eyring et al.* [2005a] (their "other PM" category) which utilize the *Petzold et al.* [2004] results. Our assessment of 0.90 Tg a^{-1} compares favorably to 0.97 Tg a^{-1} from *Eyring et al.* [2005a] and 1.13 Tg a^{-1} from *Wang et al.* [2008]. We note the significant composition differences (see Figure 11) where, for example *Eyring et al.* [2005a] assumed up to 81% SO_4^{2-}, *Wang et al.* [2008] assumed

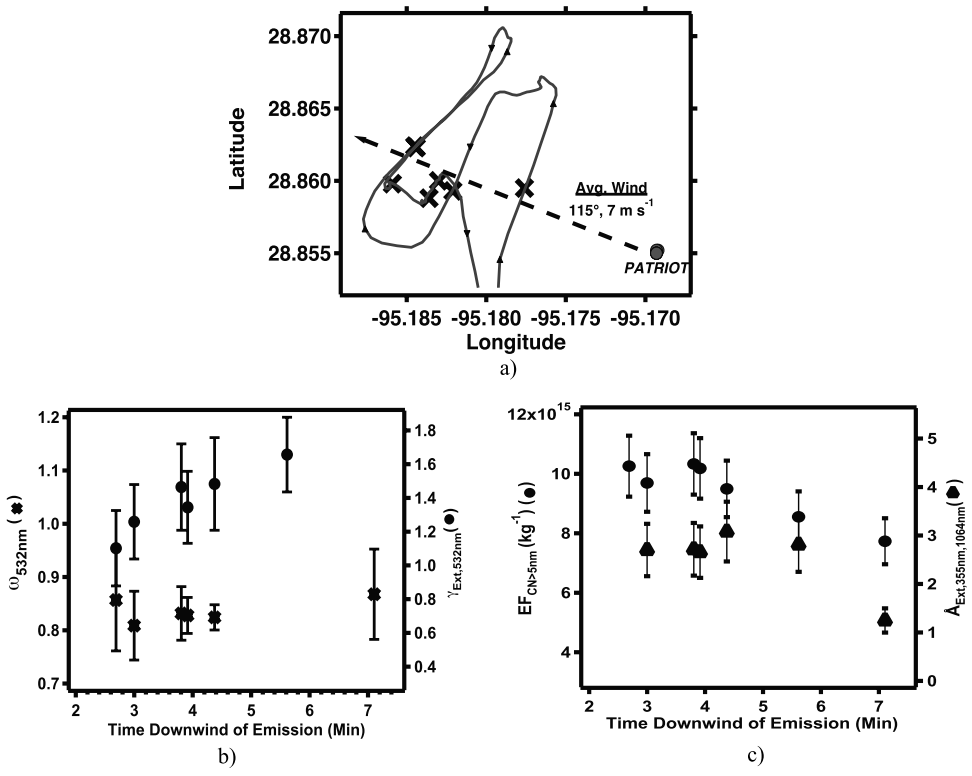

Figure 10. (a) Stationary tanker ship encounter on 8 August 2006. Map shows the latitude-longitude position of the stationary vessel, the average wind direction and speed, and the track of *Ronald H. Brown*. (b) Single scatter albedo (stars) and RH dependence (circles) as a function of time downwind of emission and (c) CN > 5 nm (circles) and extinction Ångström exponent (triangles) as a function of time downwind of emission. Not all parameters were available for all plume intersections.

Table 5. Calculated Annual Global Emissions of SO_4^{2-}, OM, and BC for Vessel Classes and Annual Fuel Consumption[a]

	Tanker	Large Cargo	Bulk Cargo	General Cargo	Noncargo	Total
FC (Mt a^{-1})	56.8	42.7	39.4	68.9	46.2	254
EF_{SO4} (kg t^{-1})	1.42	3.58	1.42	1.42	0.53	
SO_4^{2-} (Gg a^{-1})	80.7	152.9	56.0	97.8	24.5	411.9
EF_{OM} (kg t^{-1})	1.42	2.10	1.42	1.42	0.65	
OM (Gg a^{-1})	80.7	89.7	56.0	97.8	30.0	354.2
EF_{BC} (kg t^{-1})	0.38	0.60	0.38	0.38	0.97	
BC (Gg a^{-1})	21.6	25.6	15.0	26.2	44.8	133.2
Total (Gg a^{-1})	183.0	268.2	127.0	221.8	99.3	899.3

[a]FC, fuel consumption. For 2001 from *Eyring et al.* [2005a].

31% SO_4^{2-}, and this study observed an average of 46% SO_4^{2-}. Each of these studies used different methods to obtain the results. *Eyring et al.* [2005a] utilize estimates of global PM and then define PM composition through the composition results of test bed studies on a single engine [*Petzold et al.*, 2004]. This is potentially a major source of difference with this study, as test bed studies may not best represent the composition of emissions once they are diluted into the atmosphere. The results of *Wang et al.* [2008] are based on average emission rates combining past testing of in-service marine engines and some test bed results from studies over the past 20 years [*Cooper*, 2003]. These studies produced rather limited detail on BC specifically and PM speciation in general before the recent work focused on composition. In the study by *Corbett and Koehler* [2003] and related inventory studies, available emissions rate data was partitioned among PM species partly on the basis of combustion principles and consumption statistics of lubricating oils. The results presented here, represent directly measured emission factors from between 0.5 and 15 min after emission, combined with estimates of global fuel usage [*Eyring et al.*, 2005a]. In the data from this study, differences in SO_4^{2-} emission factors may arise from secondary SO_4^{2-} production. As mentioned previously, most marine engines are tuned to reduce the impact of corrosive sulfur-containing compounds within the engine and exhaust system, and as such sulfur is predominantly released as SO_2. A few percent of sulfur emissions are released as SO_3 that is assumed to quickly convert to direct SO_4^{2-} PM. Figure 12 shows, for this study, that this percentage is variable between 1 and 8% (average of 2.85%), contributing a large amount of variability to the "direct" PM emission. However, Figure 12 also shows what appears to be a relationship ($R^2 = 0.45$) between this fraction and the time downwind of emission of the sulfur from the stack. This may be evidence of fast oxidation of SO_2 to secondary SO_4^{2-} (20–30% h^{-1}) If so, these conversion rates are much faster than the conversions measured in coal-fired power plant plumes (e.g., $\sim$ 10% h^{-1} [*Brock et al.*, 2003]). The availability of highly oxidized copollutants like NO_X can increase the rates at which gaseous emissions oxidize. *Dominguez et al.* [2008] observed fast oxidation of ship-sourced SO_2 on sea salt particles, which may also contribute to the enhanced oxidation rates observed. Given that these data cannot independently establish whether the variability is due to the direct emission or secondary formation, it is critical to consider this uncertainty is assigning a direct SO_4^{2-} PM burden from shipping. From this discussion it might be expected that the results of *Eyring et al.* [2005a] would provide a lower limit to SO_4^{2-} emission. This is because their calculations were based on test bed studies, which should not allow for secondary SO_4^{2-} formation. However, because the contribution of SO_4^{2-} is $\sim$81% in the *Eyring et al.* [2005a] study, while our results show 46% SO_4^{2-}, we conclude that the compositional differences are related to the fact that the >200 vessels sampled better present an average PM composition than the test bed studies of a limited number of engines.

4.2. Expected Effects of Recently Adopted Fuel Sulfur Regulations

[38] Fuel sulfur content is one of the properties of shipping fuel that has been targeted for regional and global regulation through Annex VI to the International Convention on the Prevention of Pollution from Ships (MARPOL). Annex VI regulates sulfur emissions in two ways. First, it establishes a global cap for the sulfur content of fuel used on board ships. Second, it provides for the establishment of sulfur Emission Control Areas (ECAs), which require vessels to burn low-sulfur fuel within these areas; two such areas, have been established in the North and Baltic Seas. In 2008 the parties to MARPOL Annex VI approved vastly stricter sulfur emission control regulations for the global cap and for ECAs. These 2008 amendments contain changes to percentage limits, culminating in requirement that the sulfur content of on board fuel be limited to 0.5% starting 1 January 2020; a reduction from the 4.5% from Annex VI adopted in 1997. The sulfur content of fuels required in

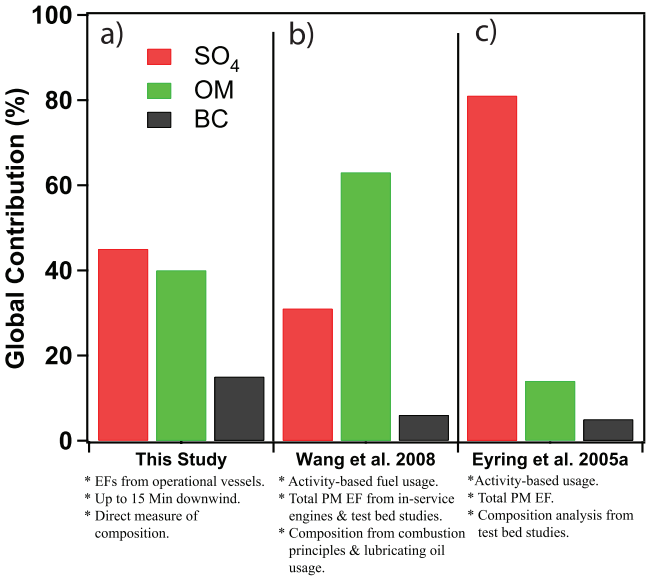

Figure 11. (a) PM compositions, comprising SO_4^{2-}, OM, and BC, as reported in this study (0.90 Tg a^{-1}) using fuel usage from *Eyring et al.* [2005a], (b) reported by *Wang et al.* [2008] (1.13 Tg a^{-1}), and (c) reported by *Eyring et al.* [2005a] (0.97 Tg a^{-1}). Figures exclude ash and SO_4-bound water. Our results suggest a larger fraction of BC relative to SO_4^{2-} and OM. A brief summary of the methods for each study is provided in the text below the figure.

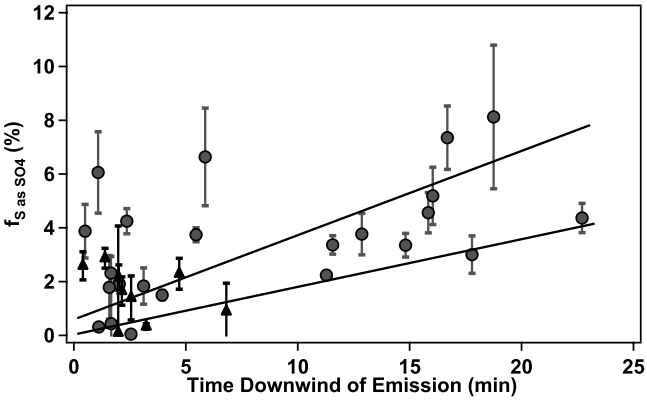

Figure 12. Fraction of total fuel sulfur converted to sulfate relative to time downwind of emission. Solids lines are estimated minimum (20%) and maximum (30%) conversion rates. Circles indicate SSD vessels, and triangles indicate MSD vessel. (Slope = 1.0, Int = 2, and $R^2 = 0.45$.)

ECAs is also amended to be more stringent, requiring that the sulfur content of fuel used in these areas are not to exceed 0.10% starting 1 January 2015. One of the major impacts of these regulations will be the reduction in PM concentrations. We show in section 4.1 that almost 50% of PM measured within a few minutes of emission are a result of fuel sulfur. Also, the potential for much more PM due to secondary formation of SO_4^{2-} from SO_2 is very large. Here we summarize some of the data related to fuel sulfur content to assess the potential changes to PM properties from the adopted fuel sulfur regulations. Table 6 summarizes the changes in average emission factors for PM properties that influence climate and air quality, or those which can be attributed to fuel sulfur content. We use a fuel sulfur content separation of >0.5% and <0.5%, simulating the Annex VI amendments. Total PM mass and number emissions could drop by up to 50%, which would be a significant change across all impacted areas. SO_4^{2-} emissions, as expected, would drop significantly (almost 2 orders of magnitude) while OM emissions are potentially cut in half. Apart from the emission reductions, there are other potential effects on particulate type and amounts in the regulated regime. Therefore, caution is required in assessing the impacts of the following changes. The average ω_{532nm} decreases by 0.2 while CCN emissions drop by an order of magnitude or more. Changes in PM composition and CCN together may have impacts on a number of areas. Most notably, even though PM mass emissions may be cut in half, PM lifetime may increase, as less of these particles form cloud droplets. An aerosol with a longer lifetime will make a larger contribution to air quality and an aerosol with a longer lifetime and stronger absorption will have a much larger impact on direct radiative forcing. If a reduction in required fuel sulfur content was introduced, the lifetime of the emitted particles would then be dictated by the chemistry of other air masses that eventually interact with shipping emissions. We also note that some of the observed relationships between fuel sulfur divisions may have contributions related to engine type, maintenance and operational characteristic, rather than purely the fuel type. This is most notable for OM (50% change) where engine type is known to play a role. BC and AMS+BC mass (total PM mass) will also be affected by engine type rather than just fuel sulfur.

5. Summary

[39] The chemical, physical and optical properties of particle emissions from more than 200 commercial shipping vessels were measured during the 2006 Texas Air Quality Study/Gulf of Mexico Atmospheric Composition and Climate Study. The data were used to compile an extensive database of the properties of particle emissions from commercial shipping. The following summarizes the major findings:

[40] 1. Particle composition is dictated by a number of factors, including fuel sulfur content, engine type, vessel activity and maintenance. Emissions of BC are strongly dependent on engine type and, as described by *Lack et al.* [2008a], for MSD engines appear correlated to CO, an indicator of combustion efficiency and maintenance. As expected SO_4^{2-} emissions are dictated by fuel sulfur content, while OM is emitted as a function of both fuel sulfur and engine type. These results are critical in understanding the mechanisms that contribute to PM mass (and subsequent air quality issues), and the results show that both fuel type and vessel activity will be a strong contributor to PM composition and mass.

[41] 2. On average SSD engines appear to emit more mass and CN than MSD engines because of higher combustion temperatures and pressures, although there was no statistical correlations between CN and fuel sulfur content or engine load. It is very likely however that all three variables (fuel type, engine type, activity) influence total CN number concentrations.

[42] 3. Strong positive correlations of fuel sulfur with OM, SO_4^{2-}, CCN, particle water uptake and particle single scatter albedo (R^2 values all above 0.6) were observed and are thus mostly attributable to fuel sulfur content; providing correlation of PM properties to a single variable. These parameters are fundamental to the impact of these emissions on climate and provide direct links between the type of fuel used and the direct and indirect radiative effect of shipping PM.

[43] 4. Correlations between PM size distributions and fuel sulfur ($R^2 = 0.64$), and nucleation mode PM and time since emission indicate that particle size (for any engine type) is mostly dictated by the mechanisms of particle formation during combustion within the engine (assessed by *Lyyranen et al.* [1999]). However, the few minutes following emission can strongly impact PM size through formation of sulfuric acid particles and coagulation of sulfuric acid with larger PM.

Table 6. Breakdown of PM Emissions According to Fuel Type

Parameter	<0.5% Sulfur Fuel	>0.5% Sulfur
EF_{SO4} (g kg^{-1})	0.06 (±0.05)	2.1 (±1.6)
EF_{OM} (g kg^{-1})	0.9 (±1.2)	1.6 (±0.7)
EF_{BC} (g kg^{-1})	1.1 (±0.8)	0.5 (±0.5)
EF_{AMS+BC} (g kg^{-1})	1.8 (±1.4)	3.3 (±1.4)
$EF_{CN>5nm}$ (kg^{-1})	1.0 (±0.7) × 10^{16}	2.0 (±1.0) × 10^{16}
EF_{CCN} (kg^{-1})	0.02 (±0.01) × 10^{16}	0.3 (±0.2) × 10^{16}
ω_{532nm}	0.35 (±0.17)	0.60 (±0.21)

[44] 5. Data from multiple interrogation of the same vessel plume shows excellent instrument precision and yields results that are consistent with plume processing studies. On the basis of this ability to measure precisely, the variability observed in the data set is attributed to vessel activity (operation characteristics), engine type and fuel type. This attribution is significant when attempting to understand emission dynamics and reduce the uncertainty in emissions from commercial vessels.

[45] 6. An assessment of global PM emission based on emission factors from this study showed that our calculated annual global contributions to PM from shipping were comparable to estimates within recent inventories. Although we calculate similar total PM mass to these inventories observations reported here show that PM composition differs from that previously assumed. This is likely due to a larger sample size in this study better representing the average than the limited statistics of previous studies. We found direct PM emissions of 0.90 Tg a^{-1} that contain 46% SO_4^{2-}, 39% OM and 15% BC.

[46] 7. Emissions by engine class (slow-, medium- and high-speed diesel engines, SSD, MSD, HSD) were found to vary, with more than twice as much OM and SO_4^{2-} emitted by SSD than MSD and HSD vessels and that more than twice as much BC emitted by MSD than SSD and HSD vessels [*Lack et al.*, 2008a].

[47] 8. High-sulfur fuels (>0.5% sulfur) emit more than twice as much PM, OM and CN as low-sulfur fuels (<0.5% sulfur). The number of CCN is significantly reduced from the combustion of low-sulfur fuels and the relative darkness of the PM increases as fuel sulfur decreases.

[48] 9. The impacts of altering fuel standards or engine technology can be assessed on the basis of the results presented here, with many of the properties having direct links to the climate and air quality impacts of shipping PM.

[49] **Acknowledgments.** This work was funded by the NOAA climate program. Thanks to the crew of the *Ronald H. Brown* and to Charles Brock, Daniel Murphy, and Lindy Johnson for helpful discussions.

References

Allan, J. D., J. L. Jimenez, P. I. Williams, M. R. Alfarra, K. N. Bower, J. T. Jayne, and H. Coe (2003), Quantitative sampling using an Aerodyne aerosol mass spectrometer: 1. Techniques of data interpretation and ERROR analysis, *J. Geophys. Res.*, *108*(D3), 4090, doi:10.1029/2002JD002358.

Bates, T. S., B. K. Lamb, A. B. Guenther, J. Dignon, and R. E. Stoiber (1992), Sulfur emissions to the atmosphere from natural sources, *J. Atmos. Chem.*, *14*, 315–337, doi:10.1007/BF00115242.

Bates, T. S., et al. (2008), Boundary layer aerosol chemistry during TexAQS/GoMACCS 2006: Insights into aerosol sources and transformation processes, *J. Geophys. Res.*, *113*, D00F01, doi:10.1029/2008JD010023.

Baynard, T., A. Pettersson, E. Lovejoy, S. Brown, D. Lack, P. Massoli, H. Osthoff, S. Ciciora, B. Dube, and A. R. Ravishankara (2007), Design and application of a pulsed cavity ring-down aerosol extinction spectrometer for field measurements, *Aerosol Sci. Technol.*, *41*(4), 447–462, doi:10.1080/02786820701222801.

Bergstrom, R. W., P. Pilewskie, P. B. Russell, J. Redemann, T. C. Bond, P. K. Quinn, and B. Sierau (2007), Spectral absorption properties of atmospheric aerosols, *Atmos. Chem. Phys.*, *7*, 5937–5943.

Berner, A., C. Lurzer, F. Pohl, O. Preining, and P. Wagner (1979), The size distribution of the urban aerosol in Vienna, *Sci. Total Environ.*, *13*, 245–261, doi:10.1016/0048-9697(79)90105-0.

Bond, T. C., and R. W. Bergstrom (2006), Light absorption by carbonaceous particles: An investigative review, *Aerosol Sci. Technol.*, *40*, 27–67, doi:10.1080/02786820500421521.

Bond, T. C., T. L. Anderson, and D. Campbell (1999), Calibration and intercomparison of filter-based measurements of visible light absorption by aerosols, *Aerosol Sci. Technol.*, *30*(6), 582–600.

Bond, T., G. Habib, and R. W. Bergstrom (2006), Limitations in the enhancement of visible light absorption due to mixing state, *J. Geophys. Res.*, *111*, D20211, doi:10.1029/2006JD007315.

Brock, C. A., et al. (2003), Particle growth in urban and industrial plumes in Texas, *J. Geophys. Res.*, *108*(D3), 4111, doi:10.1029/2002JD002746.

Buhaug, Ø., et al. (2008), Updated study on greenhouse gas emissions from ships, phase 1 report, 129 pp., Int. Maritime Organ., London.

Capaldo, K., J. J. Corbett, P. Kasibhatla, P. Fischbeck, and S. N. Pandis (1999), Effects of ship emissions on sulphur cycling and radiative climate forcing over the ocean, *Nature*, *400*(6746), 743–746, doi:10.1038/23438.

Chen, G., et al. (2005), An investigation of the chemistry of ship emission plumes during ITCT 2002, *J. Geophys. Res.*, *110*, D10S90, doi:10.1029/2004JD005236.

Cooper, D. A. (2003), Exhaust emissions from ships at berth, *Atmos. Environ.*, *37*(27), 3817–3830, doi:10.1016/S1352-2310(03)00446-1.

Corbett, J. J., and H. W. Koehler (2003), Updated emissions from ocean shipping, *J. Geophys. Res.*, *108*(D20), 4650, doi:10.1029/2003JD003751.

Corbett, J. J., C. Wang, and J. Firestone (2006), Estimation, validation, and forecasts of regional commercial marine vessel inventories, Tasks 1 and 2: baseline inventory and ports comparison, final report, 43 pp., Univ. of Del., Newark.

Corbett, J. J., C. Wang, J. J. Winebrake, and E. H. Green (2007a), Allocation and forecasting of global ship emissions, 26 pp., Clean Air Task Force, Boston, Mass.

Corbett, J. J., J. J. Winebrake, E. H. Green, P. Kasibhatla, V. Eyring, and A. Lauer (2007b), Mortality from ship emissions: A global assessment, *Environ. Sci. Technol.*, *41*(24), 8512–8518, doi:10.1021/es071686z.

DeCarlo, P. F., et al. (2006), Field-deployable, high-resolution, time-of-flight aerosol mass spectrometer, *Anal. Chem.*, *78*, 8281–8289.

Devasthale, A., O. Krüger, and H. Graßl (2006), Impact of ship emissions on cloud properties over coastal areas, *Geophys. Res. Lett.*, *33*, L02811, doi:10.1029/2005GL024470.

Dominguez, G., T. Jackson, L. Brothers, B. Barnett, B. Nguyen, and M. H. Thiemens (2008), Discovery and measurement of an isotopically distinct source of sulfate in Earth's atmosphere, *Proc. Natl. Acad. Sci. U. S. A.*, *105*, 12,769–12,773, doi:10.1073/pnas.0805255105.

Drewnick, F., et al. (2005), A new time-of-flight aerosol mass spectrometer (TOF-AMS)—Instrument and first field deployment, *Aerosol Sci. Technol.*, *39*, 637–658, doi:10.1080/02786820500182040.

Durkee, P. A., et al. (2000), The impact of ship-produced aerosols on the microstructure and albedo of warm marine stratocumulus clouds: A test of MAST hypotheses 1i and 1ii, *J. Atmos. Sci.*, *57*(16), 2554–2569, doi:10.1175/1520-0469(2000)057<2554:TIOSPA>2.0.CO;2.

Endresen, O., E. Sorgard, J. K. Sundet, S. B. Dalsoren, I. S. A. Isaksen, T. F. Berglen, and G. Gravir (2003), Emissions from international sea transportation and environmental impact, *J. Geophys. Res.*, *108*(D17), 4560, doi:10.1029/2002JD002898.

Eyring, V., H. W. Kohler, J. van Aardenne, and A. Lauer (2005a), Emissions from international shipping: 1. The last 50 years, *J. Geophys. Res.*, *110*, D17305, doi:10.1029/2004JD005619.

Eyring, V., H. W. Kohler, A. Lauer, and B. Lemper (2005b), Emissions from international shipping: 2. Impact of future technologies on scenarios until 2050, *J. Geophys. Res.*, *110*, D17306, doi:10.1029/2004JD005620.

Frick, G. M., and W. A. Hoppel (2000), Airship measurements of ship's exhaust plumes and their effect on marine boundary layer clouds, *J. Atmos. Sci.*, *57*(16), 2625–2648, doi:10.1175/1520-0469(2000)057<2625:AMOSSE>2.0.CO;2.

Heywood, J. B. (1988), *Internal Combustion Engine Fundamentals*, 930 pp., McGraw-Hill, New York.

Hobbs, P. V., et al. (2000), Emissions from ships with respect to their effects on clouds, *J. Atmos. Sci.*, *57*(16), 2570–2590, doi:10.1175/1520-0469(2000)057<2570:EFSWRT>2.0.CO;2.

Hudson, J. G., T. J. Garrett, P. V. Hobbs, S. R. Strader, Y. Xie, and S. S. Yum (2000), Cloud condensation nuclei and ship tracks, *J. Atmos. Sci.*, *57*(16), 2696–2706, doi:10.1175/1520-0469(2000)057<2696:CCNAST>2.0.CO;2.

Intergovernmental Panel on Climate Change (2007), *Climate Change 2007: The Physical Science Basis—Contribution of Working Group 1 to the Fourth Assessment Report*, Cambridge Univ. Press, Cambridge, U. K.

Ito, A., and J. E. Penner (2005), Historical emissions of carbonaceous aerosols from biomass and fossil fuel burning for the period 1870–2000, *Global Biogeochem. Cycles*, *19*, GB2028, doi:10.1029/2004GB002374.

Jayne, J. T., D. C. Leard, X. Zhang, P. Davidovits, K. A. Smith, C. E. Kolb, and D. R. Worsnop (2000), Development of an aerosol mass spectrometer for size and composition analysis of submicron particles, *Aerosol Sci. Technol.*, *33*, 49–70, doi:10.1080/027868200410840.

Jimenez, J. L., et al. (2003), Ambient aerosol sampling using the Aerodyne Aerosol Mass Spectrometer, *J. Geophys. Res.*, *108*(D7), 8425, doi:10.1029/2001JD001213.

Kasper, A., S. Aufdenblatten, A. Forss, M. Mohr, and H. Burtscher (2007), Particulate emissions from a low-speed marine diesel engine, *Aerosol Sci. Technol.*, *41*, 24–32, doi:10.1080/02786820601055392.

Kirchstetter, T. W., T. Novakov, and P. V. Hobbs (2004), Evidence that the spectral dependence of light absorption by aerosols is affected by organic carbon, *J. Geophys. Res.*, *109*, D21208, doi:10.1029/2004JD004999.

Kittiwake, (2008), Total base number (TBN), in *Fuel and Lube Oil Technical Manual* [electronic], Littlehampton, U. K. (Available at http://www.kittiwake.com/Default.aspx/Page/KB/KB/192)

Lack, D., E. Lovejoy, T. Baynard, A. Pettersson, and A. Ravishankara (2006), Aerosol absorption measurement using photoacoustic spectroscopy: Sensitivity, calibration, and uncertainty developments, *Aerosol Sci. Technol.*, *40*(9), 697–708, doi:10.1080/02786820600803917.

Lack, D. A., B. Lerner, C. Granier, T. Baynard, E. R. Lovejoy, P. Massoli, A. R. Ravishankara, and E. Williams (2008a), Light absorbing carbon emissions from commercial shipping, *Geophys. Res. Lett.*, *35*, L13815, doi:10.1029/2008GL033906.

Lack, D. A., C. D. Cappa, D. S. Covert, T. Baynard, P. Massoli, B. Sierau, T. S. Bates, P. K. Quinn, E. R. Lovejoy, and A. R. Ravishankara (2008b), Bias in filter-based aerosol light absorption measurements due to organic aerosol loading: Evidence from ambient measurements, *Aerosol Sci. Technol.*, *42*(12), 1033–1041, doi:10.1080/02786820802389277.

Lance, S., J. Medina, J. N. Smith, and A. Nenes (2006), Mapping the operation of the DMT continuous flow CCN counter, *Aerosol Sci. Technol.*, *40*, 242–254, doi:10.1080/02786820500543290.

Lauer, A., V. Eyring, J. Hendricks, P. Jockel, and U. Lohmann (2007), Global model simulations of the impact of ocean-going ships on aerosols, clouds, and the radiation budget, *Atmos. Chem. Phys.*, *7*(19), 5061–5079.

Lewis, K., W. P. Arnott, H. Moosmüller, and C. E. Wold (2008), Strong spectral variation of biomass smoke light absorption and single scattering albedo observed with a novel dual-wavelength photoacoustic instrument, *J. Geophys. Res.*, *113*, D16203, doi:10.1029/2007JD009699.

Liu, P., R. Deng, K. A. Smith, L. R. Williams, J. T. Jayne, M. R. Canagaratna, K. Moore, T. B. Onasch, D. R. Worsnop, and T. Deshler (2007), Transmission efficiency of an aerodynamic focusing lens system: Comparison of model calculations and laboratory measurements for the Aerodyne Aerosol Mass Spectrometer, *Aerosol Sci. Technol.*, *41*, 721–733, doi:10.1080/02786820701422278.

Lloyds MIU (2006), *Lloyd's Maritime Directory*, London.

Lloyd's Register (1995), *Marine Exhaust Emissions Research Program*, London.

Lyyranen, J., J. Jokiniemi, E. I. Kauppinenen, and J. Joutsensaari (1999), Aerosol characterisation in medium speed diesel engines operating with heavy fuel oils, *J. Aerosol Sci.*, *30*(6), 771–784, doi:10.1016/S0021-8502(98)00763-0.

Lyyranen, J., J. Jokiniemi, and E. Kauppinen (2002), The effect of Mg-based additive on aerosol characteristics in medium-speed diesel engines operating with residual fuel oils, *J. Aerosol Sci.*, *33*, 967–981.

Matthew, B. M., T. B. Onasch, and A. M. Middlebrook (2008), Collection efficiencies in an aerodyne aerosol mass spectrometer as a function of particle phase for laboratory generated aerosols, *Aerosol Sci. Technol.*, *42*(11), 884–898.

Petzold, A., P. Feldpausch, L. Fritzsche, A. Minikin, A. Lauer, and H. Bauer (2004), Particle emissions from ship engines, paper presented at European Aerosol Conference, Hungarian Acad. of Sci., Budapest, Hungary.

Petzold, A., J. Hasselbach, P. Lauer, R. Baumann, K. Franke, C. Gurk, H. Schlager, and E. Weingartner (2008), Experimental studies on particle emissions from cruising ships, their characteristic properties, transformation and atmospheric lifetime in the marine boundary layer, *Atmos. Chem. Phys.*, *8*, 2387–2403.

Quinn, P. K., et al. (2005), Impact of particulate organic matter on the relative humidity dependence of light scattering: A simplified parameterization, *Geophys. Res. Lett.*, *32*, L22809, doi:10.1029/2005GL024322.

Quinn, P. K., et al. (2006), Impacts of sources and aging on submicrometer aerosol properties in the marine boundary layer across the Gulf of Maine, *J. Geophys. Res.*, *111*, D23S36, doi:10.1029/2006JD007582.

Roberts, G. C., and A. Nenes (2005), A continuous-flow streamwise thermal gradient CCN chamber for atmospheric measurements, *Aerosol Sci. Technol.*, *39*, 206–221, doi:10.1080/027868290913988.

Sax, T., and A. Alexis (2007), A critical review of ocean-going vessel particulate matter emission factors, Calif. Air Resour. Board, Sacramento, Calif.

Schnaiter, M., H. Horvath, O. Mohler, K.-H. Naumann, H. Saathoff, and O. W. Schock (2003), UV-VIS-NIR spectral optical properties of soot and soot-containing aerosols, *J. Aerosol Sci.*, *34*, 1421–1444, doi:10.1016/S0021-8502(03)00361-6.

Schreier, M., A. A. Kokhanovsky, V. Eyring, L. Bugliaro, H. Mannstein, B. Mayer, H. Bovensmann, and J. P. Burrows (2006), Impact of ship emissions on the microphysical, optical and radiative properties of marine stratus: A case study, *Atmos. Chem. Phys.*, *6*(12), 4925–4942.

Schreier, M., H. Mannstein, V. Eyring, and H. Bovensmann (2007), Global ship track distribution and radiative forcing from 1 year of AATSR data, *Geophys. Res. Lett.*, *34*, L17814, doi:10.1029/2007GL030664.

Schuster, G. L., O. Dubovik, and B. N. Holben (2006), Angstrom exponent and bimodal aerosol size distributions, *J. Geophys. Res.*, *111*, D07207, doi:10.1029/2005JD006328.

Sheridan, P. J., et al. (2005), The Reno Aerosol Optics Study: An evaluation of aerosol absorption measurement methods, *Aerosol Sci. Technol.*, *39*(1), 1–16, doi:10.1080/027868290901891.

Sinha, P., P. V. Hobbs, R. J. Yokelson, T. J. Christian, T. W. Kirchstetter, and R. Bruintjes (2003), Emissions of trace gases and particles from two ships in the southern Atlantic Ocean, *Atmos. Environ.*, *37*(15), 2139–2148, doi:10.1016/S1352-2310(03)00080-3.

Slowik, J. G., et al. (2007), An inter-comparison of instruments measuring black carbon content of soot particles, *Aerosol Sci. Technol.*, *41*(3), 295–314, doi:10.1080/02786820701197078.

Stinson, K. W. (1990), *Diesel Engineering Handbook*, Bus. J., Inc., Norwalk, Conn.

Turns, S. R. (1996), *An Introduction to Combustion*, McGraw-Hill, New York.

U.S. Environmental Protection Agency (2004), *Clean air nonroad diesel—Tier 4 final rule*, edited by U. E. Otaq, Washington, D. C.

Virkkula, A., N. C. Ahlquist, D. S. Covert, W. P. Arnott, P. J. Sheridan, P. K. Quinn, and D. J. Coffman (2005), Modification, calibration and a field test of an instrument for measuring light absorption by particles, *Aerosol Sci. Technol.*, *39*(1), 68–83, doi:10.1080/027868290901963.

Wang, C., J. J. Corbett, and J. Firestone (2008), Improving spatial representation of global ship emissions inventories, *Environ. Sci. Technol.*, *42*(1), 193–199, doi:10.1021/es0700799.

J. Allan, National Centre for Atmospheric Science, University of Manchester, Manchester M13 9PL, UK.

T. S. Bates, D. Coffman, and P. K. Quinn, Pacific Marine Environment Laboratory, NOAA, 7600 Sand Point Way NE, Seattle, WA 98115, USA.

T. Baynard, Lockheed Martin Coherent Technologies, 135 South Taylor Avenue, Louisville, CO 80027, USA.

J. J. Corbett, College of Marine and Earth Studies, University of Delaware, 305 Robinson Hall, Newark, DE 19716, USA.

D. S. Covert, Atmospheric Sciences Department, University of Washington, 3737 Brooklyn Avenue NE, Seattle, WA 98195, USA.

S. Herndon and T. Onasch, Aerodyne Research, Inc., 45 Manning Road, Billerica, MA 01821, USA.

D. A. Lack, B. Lerner, E. Lovejoy, P. Massoli, A. R. Ravishankara, and E. Williams, Chemical Sciences Division, Earth System Research Laboratory, NOAA, 325 Broadway, Boulder, CO 80304, USA. (daniel.lack@noaa. gov)

B. Sierau, Institute for Atmospheric and Climate Science, Swiss Federal Institute of Technology, CHN O 16.3 Universitätstrasse 16, CH-8092 Zurich, Switzerland.